NUMERICAL INVESTIGATION OF STRESS FIELD FOR ANISOTROIC ELASTIC BONDED JOINTS

by

A. H. M. Abdullah Al Mamun

KHULNA UNIVERSITY OF ENGINEERING & TECHNOLOGY
KHULNA-9203, BANGLADESH.

Numerical Investigation of Stress Field for Anisotropic Elastic Bonded Joints

by

A. H. M. Abdullah Al Mamun

A project submitted in partial fulfillment of the requirements for the degree of Master of Science in Engineering in the Department of Mechanical Engineering

Khulna University of Engineering & Technology
Khulna 9203, Bangladesh
March, 2016

Declaration

This is to certify that the project work entitled "*Numerical Investigation of Stress Field for Anisotropic Elastic Bonded Joint*" has been carried out by *A. H. M. Abdullah Al Mamun* in the *Department of Mechanical Engineering*, Khulna University of Engineering & Technology, Khulna, Bangladesh. The project work or any part of this work has not been submitted anywhere for the award of any degree or diploma.

_____	_____
Signature of Supervisor	Signature of Candidate
Name: Dr. Md. Shahidul Islam	Name: A. H. M. Abdullah Al Mamun
Designation: Associate Professor	Roll No.: 1305501

DEDICATION

This project work is dedicated to my parents.

Approval

This is to certify that the project work submitted by *A. H. M. Abdullah Al Mamun* entitled "*Numerical Investigation of Stress Field for Anisotropic Elastic Bonded Joint*" has been approved by the board of examiners for the partial fulfillment of the requirements for the degree of *Master of Engineering* in the Department of *Mechanical Engineering*, Khulna University of Engineering & Technology, Khulna, Bangladesh in March' 2016.

BOARD OF EXAMINERS

1. Chairman

   Dr. Md. Shahidul Islam (Supervisor)
   Department of Mechanical Engineering
   Khulna University of Engineering & Technology

2. Member

   Prof. Dr. Md. Nawsher Ali Moral
   Head, Department of Mechanical Engineering
   Khulna University of Engineering & Technology

3. Member

   Prof. Dr. Khandkar Aftab Hossain
   Department of Mechanical Engineering
   Khulna University of Engineering & Technology

4. Member

   Prof. Dr. Mihir Ranjan Halder
   Department of Mechanical Engineering
   Khulna University of Engineering & Technology

5. Member

   Prof. Dr. Mohammad Rofiqul Islam (External)
   Department of Mechanical Engineering
   Rajshahi University of Engineering & Technology

Acknowledgements

At first, I would like to express my praise and gratitude to the Merciful and Almighty Allah, who makes me capable to successfully complete this study.

I would like to express my deep and sincere gratitude to my supervisor, Dr. Md. Shahidul Islam, Associate Professor, Department of Mechanical Engineering, KUET, for his encouragement, supervision and useful suggestions throughout this study. His wide knowledge and his logical way of thinking have been of great value for me. His understanding, encouraging and personal guidance have provided a good basis for the present thesis. I am really honored for the opportunity to work under his supervision.

My sincere gratitude and thanks are extended to Prof. Dr. Muhammed Alamgir, the honorable Vice- Chancellor of KUET, for the financial support given to this project without which this work could not be completed.

I would also like to express my heartfelt gratitude to Prof. Dr. Md. Nawsher Ali, Head, Department of Mechanical Engineering, KUET, for allowing me to use the facilities and supports to carry out the project in the CSM Lab.

I would also convey my sincere gratitude to the committee members: Prof. Dr. Md. Nawsher Ali, Head, Department of Mechanical Engineering, Prof. Dr. Khandkar Aftab Hossain and Prof. Dr. Mihir Ranjan Halder, Department of Mechanical Engineering, KUET. Their expert guidance and valuable comments helped me to improve my masters dissertation.

My profound gratitude is extended to Prof. Dr. Mohammad Rofiqul Islam, Department of Mechanical Engineering, RUET, for his valuable suggestions and encouragement to the project until the completion of this report.

During this work I have collaborated with many colleagues for whom I have great regard, and I wish to extend my warmest thanks to all of them who have helped me with my work in the Department of Mechanical Engineering, Khulna University of Engineering & Technology, Khulna.

I owe my special gratitude to my father, mother, brother and sister. Without their encouragement and understanding it would have been impossible for me to finish this thesis.

A. H. M. Abdullah Al Mamun

Abstract

In recent years, intelligent or smart structures and systems have drawn more and more attention. Bonded structures are playing a key role as active components in many fields of engineering and technology. Mechanical stress occurs in smart structures for mechanical or thermal loading. The stress concentrations caused by mechanical or thermal loads may lead to crack initiation and extension, and sometimes the stress concentrations may be high enough to debond the material parts. Reliable service lifetime predictions of bonded components demand a complete understanding of the debonding processes of these materials. The stress fields are one of the main factors responsible for debonding under mechanical or thermal loading. Stress singularity frequently occurs at a vertex in an interface of joints due to discontinuity of materials. Stress singularity is related to debonding and delamination at interface of the bonded joints. Different numerical methods had developed for determining the stress field in a 3D dissimilar material joint. Several studies have investigated the stress field in 3D elastic materials. Recently, some researchers proposed the solution of singular stress field and its stress intensity factors of an interfacial corner of a 2D dissimilar anisotropic material joint with crack. However, the stress field at a vertex in 3D anisotropic elastic bonded joints has not been made clear. In this study, the stress field at a vertex and interface edge has been investigated in anisotropic bonded joints.

The project was focused on the reliability of anisotropic elastic bonded joints under varying tensile load condition. In the present work, the displacement and stress distributions at the vertex and along the interface edge of the joint were determined using Autodesk Simulation Mechanical 2015 software. The activities of the project involve the use of advanced numerical techniques based on Finite Element Method (FEM). The stress field in anisotropic elastic bonded joints with different materials condition was calculated. The stress and displacement field near the vertex and interface edge was investigated using developed model and material combination. Finally, the numerical results were analyzed. The numerical results suggest that the displacement and stress distribution at the vertex and interface edge were larger than the inner portion of the joints. Therefore there is a possibility of delamination and debonding occurs near the vertex and free edge of the interface of bonded joint due to higher stress concentration.

Nomenclature

x, y, z	Ordinates of global coordinate system
r, θ, φ	Ordinates of spherical coordinate system
ξ, η, ζ	Ordinates of local coordinate system
u, v, w	Displacement components in global coordinate system
$\varepsilon_x, \varepsilon_y, \varepsilon_z$	Principal strains in global coordinate system
$\varepsilon_{xy}, \varepsilon_{yz}, \varepsilon_{xz}$	Shear strains in global coordinate system
$\gamma_{xy}, \gamma_{yz}, \gamma_{zx}$	Engineering shear strains in Cartesian coordinate system
$\sigma_x, \sigma_y, \sigma_z$	Principal stresses in global coordinate system
$\tau_{xy}, \tau_{yz}, \tau_{xz}$	Shear stresses in global coordinate system
b_i	Body forces
α, β	Parameters describing shear deformation
D	Derivative matrix
C_{ijkl}	Fourth rank tensor representing elastic constant of material
E	Young's Modulus
ν	Poisson's Ratio
ε	Column matrix of strains
σ	Column matrix of stresses
s	Elastic compliance matrix of material
W	Strain energy density function
e_i	Unit vector
Q	Matrix of direction cosines
t_i	Surface traction
N_i	Shape function
$f( )$	Representing any arbitrary function
q	Matrix of nodal displacement
J	Jacobian matrix

J^{-1}	Inverse of Jacobian matrix
B	Strain-displacement matrix
k	Element stiffness matrix
K	Integrated stiffness matrix
f_b	Integrated body force
f_t	Integrated traction force
A	Representing area
V	Representing volume

Contents

LIST OF TABLES

LIST OF FIGURES

CHAPTER I

Introduction

1.1 General

In recent years, intelligent or smart structures and systems have drawn more and more attention. Bonded structures are playing a key role as active components in many fields of engineering and technology. Mechanical stress occurs in smart structures for mechanical or thermal loading. The stress concentrations caused by mechanical or thermal loads may lead to crack initiation and extension, and sometimes the stress concentrations may be high enough to debond the material parts. Reliable service lifetime predictions of bonded components demand a complete understanding of the debonding processes of these materials. When two materials are joined, a free-edge stress singularity usually develops at the intersection of the interface and the free surface. The stress fields are one of the main factors responsible for debonding under mechanical or thermal loading. Stress singularity frequently occurs at a vertex in an interface of joints due to a discontinuity of materials. Stress singularity is related to debonding and delamination at interface of the bonded joints. Different numerical methods have developed for determining the stress field in a 3D dissimilar material joint.

1.2 Finite Analysis Method

In the engineering analysis, many problems can be explained by the differential equation or integral equation. For example, the calculation of heat transfer on the car engine can be explained by the differential equation of heat balance. However, it is very difficult to find the exact solution of the differential equation and integral equation. So the approximation solution is needed. The basic approximate method is finite difference method. It is easy to study and understand but cannot determine and analyze the complex shape problem. According to this problem, the new method, finite element method (FEM) is invented and developed. In the finite element method, a distributed physical system to be analyzed is divided into a number (often large) of discrete elements. The complete system may be complex and irregularly shaped, but the individual elements are easy to analyze.

1.3 Dissimilar Material Joints

Actually, dissimilar material joint has been used in many industrial products such as vehicles, medical instruments and electrical devices. A mismatch of material properties and the

coefficient of thermal expansion cause the failure of joints. The durability and performance of joints are affected by several parameters such as material property, temperature cycle, external and internal forces. The examples of dissimilar material joints in engineering applications are shown in Fig.1.1.

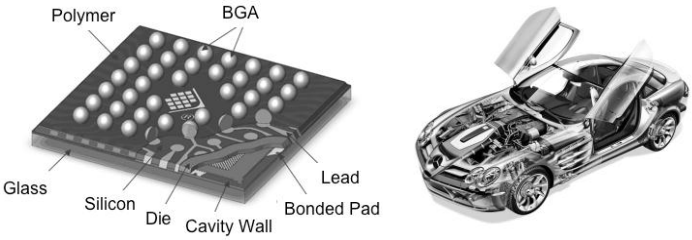

Electronic packaging Vehicle

Figure 1.1: Dssimilar material joints in engineering applications

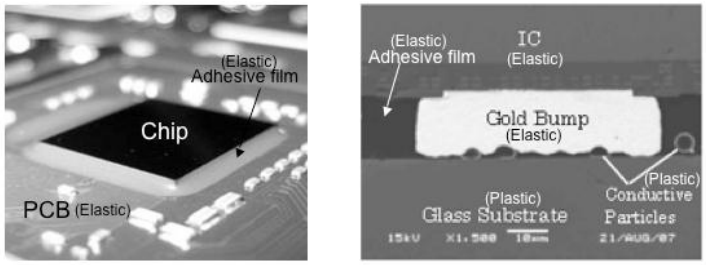

Figure 1.2: Adhesive bonded joints of electronic packaging

Dissimilar materials can be joined using many methods, such as mechanical connection (Screw/Nut & Bolt/Rivet), welding methods (friction and diffusion), gluing or chemical bonding, brazing procedures and soldering processes.

In an electronic packaging, soldering and adhesive joining methods have been widely used. Figure 1.2 shows solder joints and adhesive bonded joints using in electronic devices. These joints are composed of elastic and plastic materials. Electronic parts are mounted for a flow of electric current. Most problems in electronic devices are caused from the failure of joint in the mounting part. Many researchers have analyzed the failure of solder joints in flip chip bonding [1-4]. The characteristic of stress on the interface of a dissimilar material joint becomes an important factor for determining the durability of joint and has investigated by many authors. When dissimilar materials are jointed and an external force is applied to those, stresses always increase as approaching to the free edges of dissimilar material joint interface, which is referred to as stress singularity field. The stress singularity field may cause delamination or crack propagation at the singular points of the interface.

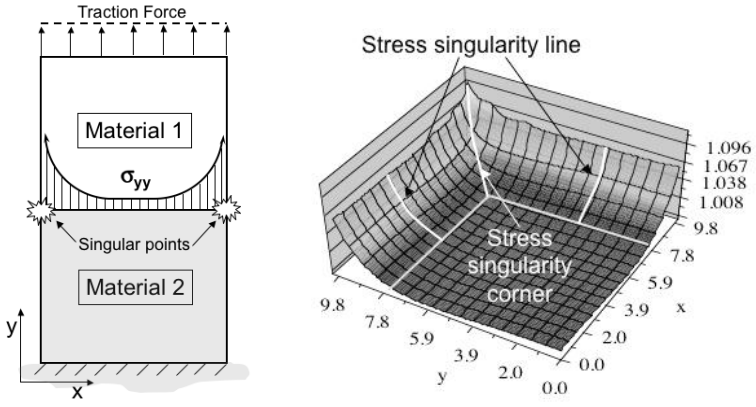

2D bonded structure 3D bonded structure

Figure 1.3: The stress singularities exist nearly the vertex of bonded joint

Figure 1.3 (left) shows the stress σ_{yy} rapidly increases near the singular points of the free edge interface in a two-dimensional dissimilar material joint under a traction force. Figure 1.3 (right) shows the stress profile on the interface in a three-dimensional dissimilar material joint. The stress rapidly increases near singularity lines and drastically increases near a singularity corner.

1.4 Anisotropic Elasticity

Anisotropic materials are materials whose properties are directionally dependent. Unlike isotropic materials that have material properties identical in all directions, anisotropic material's properties such as Young's Modulus, change with direction along the object. Common examples of anisotropic materials are wood and composites. Directionally dependent physical properties of anisotropic materials are significant due to the affects it has on how the material behaves. For example, in the case of fracture mechanics, the way the microstructure of the material is oriented will affect the strength and stiffness of the material in various directions therefore affecting direction of crack growth. Anisotropic materials, naturally and man-made, are used in multiple areas of study. Some examples are Magnetic anisotropy in which the magnetic field is oriented in a preferred direction, anisotropic heat conduction that is dependent on the geometry and or anisotropic material. Anisotropic materials are also a result of manufacturing of materials such as a rolling or deep-drawing process. Composites and other materials are used and altered for specific applications. Based on Linear Elasticity, stress and strain of a material is related by the constitutive, or stiffness matrix. This relationship is defined by the equations and matrices below using Hooke's Law:

$$\sigma_{ij} = C_{ij}\varepsilon_{ij} \quad \text{and} \quad \varepsilon_{ij} = S_{ij}\sigma_{ij}$$

Where σ_{ij} and ε_{ij} describe the stress and strain components, *i* indicating direction of normal to plane and *j* indicating direction of component. C_{ij} is the material's stiffness or Elastic Constant and S_{ij} is the compliance or inverse of C_{ij}. The stiffness tensor is a fourth order tensor C_{ijkl} that is originally consisting of 89 components. The Compliance matrix is 1/stiffness and will follow the same concepts to be described. However due to symmetry *ijkl = jikl* and *ijkl = ijlk* and other relationships as shown in the reduced matrix below, simplifies to 36 components. The relationship of shear components *ij = ji* reduces this further. By this concept one can see that the 6 diagonal components are related to the normal stress and strains: 36 - 6 = 30. The remaining 30 can be divided by two with the shear relationship 30/2 = 15 independent components. Thus the 6 + 15 components of the matrix results to 21 independent components of the stiffness/compliance matrix for anisotropic materials.

1111	1112	1113	1121	1122	1123	1131	1132	1133
1211	1212	1213	1221	1222	1223	1231	1232	1233
1311	1312	1313	1321	1322	1323	1331	1332	1333
2111	2112	2113	2121	2122	2123	2131	2132	2133
2211	2212	2213	2221	2222	2223	2231	2232	2233
2311	2312	2313	2321	2322	2323	2331	2332	2333
3111	3112	3113	3121	3122	3123	3131	3132	3133
3211	3212	3213	3221	3222	3223	3231	3232	3233
3311	3312	3313	3321	3322	3323	3331	3332	3333

iikk 9/1 = 9 ijkk or iikl 36/2 = 18

→ ijkl jikl ijlk or jilk 36/4 = 9

9 + 18 + 9 = 36

$$\begin{Bmatrix}\sigma_{11}\\ \sigma_{22}\\ \sigma_{33}\\ \sigma_{12}\\ \sigma_{13}\\ \sigma_{23}\end{Bmatrix} = \begin{bmatrix} C_{11} & C_{12} & C_{13} & 0 & 0 & 0 \\ & C_{22} & C_{23} & 0 & 0 & 0 \\ & & C_{33} & 0 & 0 & 0 \\ & & & C_{44} & 0 & 0 \\ & & & & C_{55} & 0 \\ & & \textit{symm.} & & & C_{66} \end{bmatrix} \begin{Bmatrix}\varepsilon_{11}\\ \varepsilon_{22}\\ \varepsilon_{33}\\ 2\varepsilon_{12}\\ 2\varepsilon_{13}\\ 2\varepsilon_{23}\end{Bmatrix}$$

It has been recognized that deformation behavior of many materials depends upon the orientation; that is the stress-strain response of a sample taken from the material in one direction will be different if the sample were taken in a different direction. The term anisotropic is generally used to describe such behaviors. Early investigators of these phenomena were motivated by the response of naturally occurring anisotropic materials such as wood and crystalline solids. Today, extensive use of engineered composites has brought

forward many new types of fiber and particle reinforced materials is very important for proper use of these new high performance materials in structural application.

1.5 Stress Singularity

The stress singularity was briefly explained in the previous section. Stress singularity is basically a mathematical definition for stress. As we know, when radial distance from the origin, *r* tends to zero stress tends to infinity. It is termed as singular stress or stress singularity. It can be found on points in which a load is directly applied. This can be best explained by the following example.

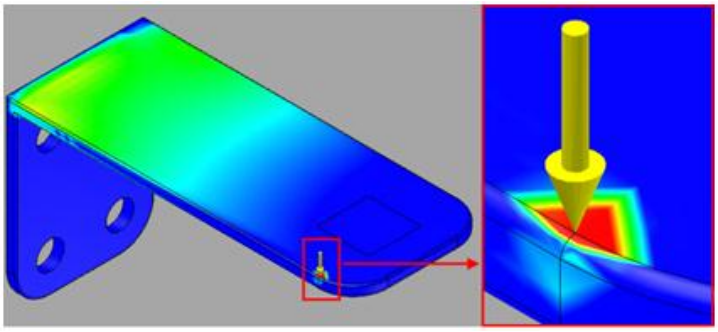

Figure 1.4: Stress singularity field

The above bracket has a high stress around the force applied on a point. This stress can be considerably higher than the operational stress. This phenomenon is known as stress singularity. There are lots of papers related to stress singularity.

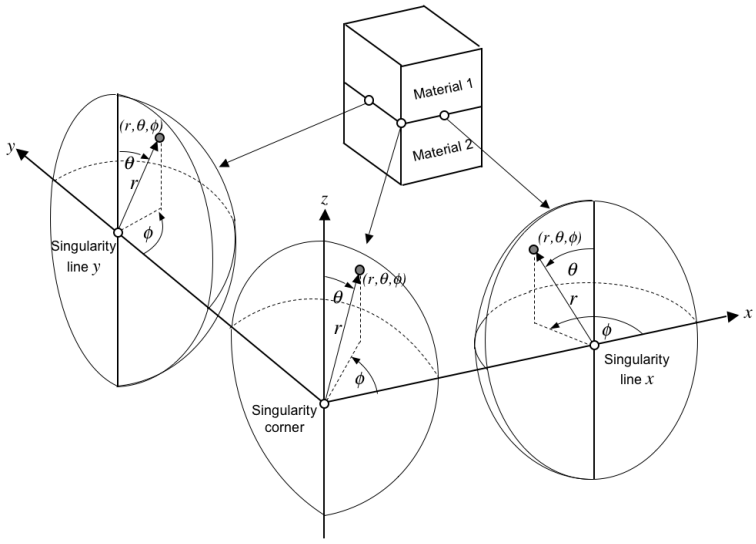

Figure 1.5: Geometry of 3D material joint using spherical coordinates at singularity lines

The stress singularity occurs not only at the vertex of the three-dimensional structure of dissimilar materials but also along the intersection of the interface with the free surface, and the cross line of the interface is referred as a stress singularity line. Figure 1.5 shows that singular points are located at the singularity corner and along the singularity lines x and y. Stress fields around these singular points can be defined by spherical coordinates (r, θ, ϕ). The singular points are located continually along the singularity lines.

1.6 Electronic Packaging

The many different functions of semiconductor devices are made possible by integrated circuits, which are built into the surface of a silicon chip (bear chip) using a complex process. If these chips could be used in unmodified form, packaging would be unnecessary, and the cost of chips reduced. However, because silicon chips are very delicate, even a tiny speck of dust or drop of water can hinder their function. Light can also cause malfunctions. To combat these problems, silicon chips are protected by packages.

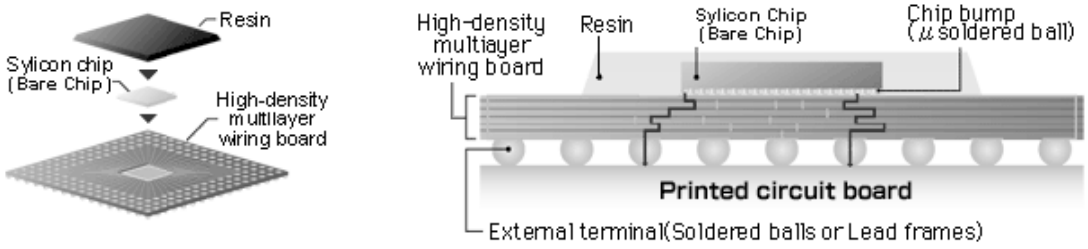

Figure 1.6: Electronic packaging (example for FCBGA)

Packages perform the following functions.

1.6.1 Protecting from the external environment: Moisture and dust in the air are direct causes of semiconductor device defects, in addition to vibration and shock. Lighting and magnets may also cause malfunctions. One function of a package is to prevent such problems from occurring. In other words, packages shut out external influences and serve to protect silicon chips.

1.6.2 Enabling electrical connectivity: If silicon chips are simply wrapped in the package material to protect them from the external environment, they will be unable to exchange signals with the outside. Attaching metal "legs" consisting of lead frame (soldered balls in the case of BGA) therefore allows signals to be sent to semiconductor devices from outside, and the results of processing accessed.

1.6.3 Heat radiation: Silicon chips heat up when in operation. If the temperature of the actual chip becomes too high, the chip will malfunction. However, packages can effectively release this heat. And in the case of semiconductor devices that give off especially high levels of heat, such as the CPUs mounted in a PC, heat release can be induced by mechanisms such as a heat sink or cooling fan.

1.6.4 Improving functionality: Semiconductor devices demonstrate their functions once directly mounted on printed circuit boards. The delicacy of circuits built into silicon chips means they cannot easily be handled, due to their minute size. Terminals are therefore enlarged to a size that makes them much easier to handle, and mounted on the chips with more space in between, allowing them to be connected to a printed circuit board.

1.7 Objectives of the Research Work

Many authors have been developed the analysis of stress field at singular points in dissimilar elastic material joint using FEM methods as the same as that in the experiment. Several authors have also been introduced the analysis of stress field of elastic material using BEM method.

The purpose of this study is to obtain a better understanding of the problem of singularity at a vertex in anisotropic dissimilar material joints. The present analysis is carried out with the help of Autodesk Simulation Mechanical 2015 Software. The FEM is used for stress field analysis at vertex of three-dimensional anisotropic elastic bonded joints. The main objectives of this project are:

(1) To determine the displacement and stress distribution at the vertex and along the interface edge of the joint.
(2) To investigate the stress singularity field of anisotropic elastic bonded joints.
(3) To study the effect of tensile load on bonded joints.
(4) To analyze the delamination and debonding process of bonded structure.

CHAPTER II

Literature Review

2.1 General

Industrial products such as electronic devices and heat endurance parts are composed of dissimilar materials. Most materials become the elastic properties when external forces or a variation of temperature applied to these materials. A mismatch of material properties causes a failure at the free edge of joint because a stress concentration occurs along the free edge of interface especially at the vertex of joint. The failure of joint has been investigated by experiments and numerical analysis. Recently, the numerical analysis has become important because the numerical analysis results can be used instead of the experimental results. As the same as the experiment, the three-dimensional numerical analysis and the elastic material properties should be considered. Over sixty years ago, many authors have determined the characteristics of singular stress fields at singular points in two-dimensional numerical analysis for elastic and elastic dissimilar material joints. Recently, some researchers have extended the two-dimensional numerical analysis to three-dimensional numerical analysis for elastic dissimilar material joints using the numerical methods that has the small number of element.

2.2 Review of the Past Study

The study on this field has been carried out step by step. William [5] used the numerical analysis for analyzing stress singularities in infinite wedges and applied to the analysis of stress distribution at the vicinity of a crack tip [6]. Zak and Williams [7] used eigen functions for analyzing stress singularity field at a crack tip perpendicular to a bi-material interface. A real part of eigen value was within the range of 0 to 1, and expressed a relationship between stress distribution and the order of stress singularity at the crack tip. Aksentian [8] determined eigen values and eigen vectors at a singular point in plane intersecting a free edge of the interface in three-dimensional dissimilar joints. In 1969, Dundurs [9] discussed a paper on an edge-bonded joint that are subjected to specify surface tractions. He proposed the well-known parameters namely, Dundurs' parameters, a and b. The order of stress singularity for two-dimensional dissimilar materials could be represented consistently on Dundurs composite plane regardless of different combinations of elastic properties and Poisson's ratios. Dundurs showed how to reduce the number of composite material parameters involved from three to two.

Bogy [10] and Bogy and Wang [11] analyzed the plane problem of bonded dissimilar material wedges under a surface traction and determined the stress singularity field at the corner in the wedge. They determined the order of stress singularity depending on material constants and the angle of wedges. Kawai, Fujitani and Kobayashi [12] performed the stress analysis at a conical surface pit and applied Williams' method to a three-dimensional crack problem. Numerical analysis of characteristic roots for conical pit problem was analyzed for determining eigen values at the vertex of conical pit. Kawai, Fujitani and Kumagai [13] investigated the stress singularity of a three-dimensional surface crack, especially its peculiar behavior at the free end of the crack front line, and then analyzed the surface crack problem by employing spherical coordinates. Benthem [14] determined the eigen values using eigen analysis and examined stress components of Cartesian coordinates at the vertex of a quarter-infinite crack in a half-space for various Poisson's ratios.

Dempsey and Sinclair [15] considered the characteristic of singular behavior in two-dimensional wedges. They focused on a single-material wedge and a composite material wedge. Airy stress function was used for determining stress and displacement fields for all wedge angles. Then, in 1995, Dempsey [16] examined particular cases in which power-logarithmic singularities occur.

Bazent and Estenssoro [17] and Yamada and Okumura [18] developed a finite element analysis for solving eigen value equation to determine directly the order of stress singularity and the angular variation of the stress and displacement fields. This eigen analysis was used to evaluate the order of singularity at a point where a crack meets a free surface in an isotropic material. Then, Pageau, Joseph and Biggers [19] adapted the eigen analysis based on a finite element for analyzing the inplane deformation of wedges and junctions that composed of anisotropic materials. The stress and displacement fields were obtained from eigen formulation for real and complex orders of stress singularity. Pageau and Biggers [20] applied to analyze the joints including fully bonded multi-material junctions intersecting a free edge as well as materials containing crack intersecting a free edge. This study showed that the order of singularity in the three-dimensional stress field could be accurately determined with a relatively small number of elements. Pageau and Biggers [21] determined the order of stress singularity and the angular variation of the displacement and the stress fields around the singular points in plane intersecting a wedge front in the three-dimensional anisotropic material structures using the two-dimensional displacement formulation under a plane strain assumption.

Koguchi [22] examined the order of stress singularity at a vertex and also along the stress singularity line between two isotropic materials in joints using eigen analysis. The stress distributions around the vertex were determined using a boundary element method (BEM). Koguchi [23] determined the intensity of singularity by fitting the stress profile that obtained from BEM analysis with a least square method. Leblond and Leguillon [24] examined the asymptotic behavior of the stress intensity factors near an angular point of a crack front in homogeneous isotropic elastic body in the cases of the crack existing at a notch or a corner.

Dimitov, Andra and Schnake [25, 26] presented the three-dimensional eigen analysis that used Arnoldi method. This method needs only the small-banded matrix when compared with normally used determinant method. The order of singularities at corners and free edges of the interface in laminate composite material joints were determined using the eigen analysis. Lee and Im [27] used a two-state M-integral for computing the near-tip stress intensities around three-dimensional wedges and used an eigen analysis for determining eigen values and eigen vectors.

Apel, Leguillon, Pester and Yosibash [28] determined edge singularity by the use of three-dimensional Williams' expansion. The edge stress intensity factors along the reentrant wedge front were determined using a quasi-dual function method. Yosibash, Omer and Dauge [29] and Omer and Yosibash [30] computed the complex eigen function by using a *p*-version finite element method and examined the edge stress intensity factors at the edge vicinity in three-dimensional anisotropic multi-material interfaces using a quasi-dual function method. The reviewed papers above can be summarized as below:

Stress distributions and the order of stress singularity were determined at crack tips and singular points in bonded joint using two-dimensional numerical models. The numerical methods that have the small number of element have been popularly used for determining the stress singularity in three-dimensional crack and bonded joint. Many authors individually determined the intensities of singularity at a corner singular point or along the free edges of the interface in a three-dimensional dissimilar material joint. However, the intensity of singularity should be considered at the singularity corner together with that along the free edge of the interface in a three-dimensional material joint. Therefore, the aim of the present research is to determine the stress and displacement field at a vertex and the interface edge in three-dimensional anisotropic elastic dissimilar material joint.

CHAPTER III

Method of Analysis

3.1 Finite Element Method (FEM)

Behaviors of natural phenomena that are surrounding the human can be expressed by the physical rules and numerical equations such as differential equation or integral equation. Normally the differential equations for determining some physical problems are easily expressed but the exact solutions of those problems are most difficultly determined by analytical method. Thus the approximation solution is required. The first popular approximation solution is a finite difference method (FDM). The finite difference method is the method for approximating numerical results by the system of differential equations. This method is easy to understand and write computer program for solving the approximated results. However, The FDM method is restricted to handle the rectangular shapes and simple alterations. It is difficult to define the boundary conditions and to use for complex shape problems. So it is useless for developing the advanced problems.

As the reasons above, the method that is higher quality than FDM approach called a finite element method (FEM) is used to be a choice for determining approximate solution of partial differential equations as well as of integral equations. FEM originated in the civil and aeronautical engineering for solving the complex elastic and structural analysis problems. Alexander Hrennikoff [31] and Richard Courant adapted the continuous domains of FDM solution to a set of discrete sub-domains. Hennikoff divided the domain by using a lattice analogy while Courant divided the domain into finite triangular subregions for solution of second order elliptic differential equations [32]. After that, in 1953, Clough [33] developed in plane stiffness matrices for 2-dimensional plate with corner connections for a delta wing structure. He used both of rectangular and triangular plates as the sub domain and successfully studied of assemblages of triangular plate. He called these plates that “elements”. Mathematical results were compared with the experiment results. Then he found that the mathematical results approached to the experiment results when the triangular elements were refined [34]. His work for stress analysis was reported in reference [35]. In this paper, Clough gave the name for the procedure that the FEM because it deals with finite components rather

than differential slices. His further works using FEM were written in references [36-37]. For a short time, FEM has been widely used to the variety of engineering. Furthermore, in 1965, NASA requested him to develop the finite element software NASTRAN. Figure 3.1 shows the comparison of the finite difference model and the finite element model for approximating the numerical results in a typical plate. FEM has ability to handle complicated geometries of analysis in structural mechanics. Its ability allows to solving many factor in engineering fields such as deformation, stresses-strains in solid bodies or dynamics of structure.

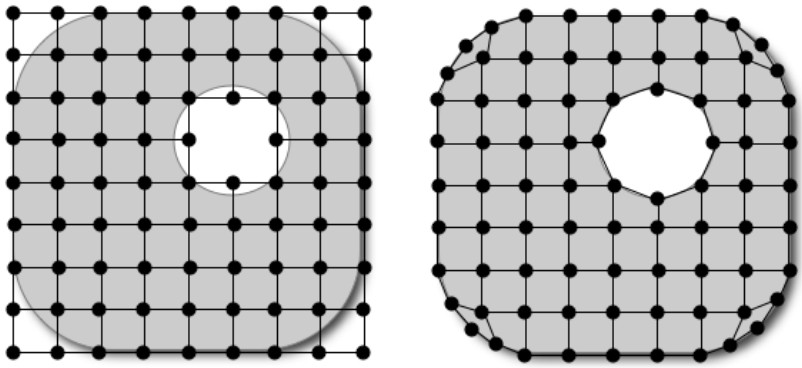

Figure 3.1: (Left) FDM model, (Right) FEM model

In fact, a physical problem is composed of infinite values of unknown parameters. The concept of FEM is to change from the infinite values to the finite values of unknown parameters by replacing the shape of physical problem with the assembly of elements as shown in Fig. 3.1 (right). Each element is connected to each other via the connecting point (node) of element. FEM formulations that depend on the differential equation of the problem are individually formed in each element. After that, the FEM formulations in each element are assembled to be a main equation. It seems to assemble all elements together. Then the boundary conditions of the problem are taken in to the main equation. Finally, the unknown parameters at nodes are known by solving the main equation. In the mechanical engineering, unknown nodal parameters are defined by displacements at these nodes. The accuracy of approximate results depends on the number and size of element and the interpolation functions in each element.

3.2 Total Potential Energy for Analysis of Solid Mechanics Problems

The FEM formulation can be expressed from the total of potential energy at equilibrium condition. The total of potential energy (J^*) is in the form of the following equation.

$$J^* = U^* + W^* \tag{3.1}$$

Where U^* is the internal strain energy. For the linear elastic material, the internal strain

energy of the system that has a volume (V) is given by

$$U^* = \frac{1}{2}\int_V [\varepsilon]^T [C][\varepsilon] dV \tag{3.2}$$

Where $[\varepsilon]$is strain matrix and $[C]$is elasticity matrix of modulus W^* is the potential energy due to external forces such as body force (F) on a volume (V) and surface traction on a surface (S). The potential energy due to external forces is simply given by

$$W^* = -\int_V \left(F_x u + F_y v + F_z w\right) dV - \int_S \left(T_x u + T_y v + T_z w\right) dS \tag{3.3}$$

and it will be $W^* = -\int_V [U]^T \{F\} dV - \int_V [U]^T \{T\} dS$ (3.4)

Where the vector [U] is the virtual displacements (u, v, w) in directions (x, y, z) of the Cartesian coordinate. Here the total of potential energy is obtained by substituting Eqs. (3.2) and (3.4) into Eq. (3.1). It becomes as the following equation.

$$J^* = \frac{1}{2}\int_V [\varepsilon]^T [C][\varepsilon] dV - \int_V [U]^T \{F\} dV - \int_S [U]^T \{T\} dS \tag{3.5}$$

The displacement formulation for an e nodes element is expressed as the following equation.

$$u_i = \sum_{n=1}^{e} N_n \bar{u}_{in} \tag{3.6}$$

Where u_i is the displacement in direction i. $\bar{u}_{in}$ is the displacement at node n associated with direction i. N_n is the interpolation function at node n.

Using the equation above, the vector of strain in Eq. (3.5) can be expressed with the form of displacement as follows:

$$\{\varepsilon\} = \begin{Bmatrix} \varepsilon_x \\ \varepsilon_y \\ \varepsilon_z \\ \gamma_{xy} \\ \gamma_{yz} \\ \gamma_{zx} \end{Bmatrix} = \begin{Bmatrix} \frac{\partial u}{\partial x} \\ \frac{\partial v}{\partial y} \\ \frac{\partial w}{\partial z} \\ \frac{\partial u}{\partial y} + \frac{\partial v}{\partial x} \\ \frac{\partial v}{\partial z} + \frac{\partial w}{\partial y} \\ \frac{\partial u}{\partial z} + \frac{\partial w}{\partial x} \end{Bmatrix} = [B]\{\bar{U}\} \tag{3.7}$$

Where [B] is the differential operator matrix in the form of the differential of interpolation

functions. The total of potential energy equation becomes

$$J^* = \frac{1}{2}\int_V \{\bar{U}\}^T [B]^T [C][B]\{\bar{U}\}dV - \int_V \{\bar{U}\}^T [N]^T \{F\}dV - \int_S \{\bar{U}\}^T [N]^T \{T\}dS \tag{3.8}$$

The total of potential energy is minimum when it is being in the equilibrium condition. The variation of the total of potential energy (δJ^*) in this state must be stationary for variation of the displacement. It means that the variation of the total of potential energy becomes zero as equation below:

$$\delta J^* = \frac{\partial J^*}{\partial \bar{U}} = \frac{\partial \left(U^* + W^*\right)}{\partial \bar{U}} = 0 \tag{3.9}$$

The finite element equation of the total of potential energy is expressed as

$$J^* = \frac{1}{2}\{\bar{U}\}^T [K^*]\{\bar{U}\} - \{\bar{U}\}^T \{F_B\} - \{\bar{U}\}^T \{F_t\}$$

$$\frac{\partial J^*}{\partial U} = [K^*]\{U\} - \{F_B\} - \{F_t\} = 0 \tag{3.10}$$

and it is simply given by

$$[K^*]\{U\} = \{F_B\} + \{F_t\} \tag{3.11}$$

Where

$$[K^*] = \int_V [B]^T [C][B]dV \tag{3.12}$$

$$\{F_B\} = \int_V [N]^T \{F\}dV \tag{3.13}$$

$$\{F_t\} = \int_S [N]^T \{T\}dS \tag{3.14}$$

$[K^*]$ is the stiffness matrix and $\{F_B\}, \{F_t\}$ are the load vectors form body forces and traction forces, respectively. The matrix [*B*] for a hexahedron element is expresses as follows:

$$[B]=\begin{bmatrix} \frac{\partial N_1}{\partial x} & 0 & 0 & \frac{\partial N_2}{\partial x} & 0 & 0 & \mathsf{L} & \frac{\partial N_8}{\partial x} & 0 & 0 \\ 0 & \frac{\partial N_1}{\partial y} & 0 & 0 & \frac{\partial N_2}{\partial y} & 0 & \mathsf{L} & 0 & \frac{\partial N_8}{\partial y} & 0 \\ 0 & 0 & \frac{\partial N_1}{\partial z} & 0 & 0 & \frac{\partial N_2}{\partial z} & \mathsf{L} & 0 & 0 & \frac{\partial N_8}{\partial z} \\ \frac{\partial N_1}{\partial y} & \frac{\partial N_1}{\partial x} & 0 & \frac{\partial N_2}{\partial y} & \frac{\partial N_2}{\partial x} & 0 & \mathsf{L} & \frac{\partial N_8}{\partial y} & \frac{\partial N_8}{\partial x} & 0 \\ \frac{\partial N_1}{\partial z} & 0 & \frac{\partial N_1}{\partial x} & \frac{\partial N_2}{\partial z} & 0 & \frac{\partial N_2}{\partial x} & \mathsf{L} & \frac{\partial N_8}{\partial z} & 0 & \frac{\partial N_8}{\partial x} \\ 0 & \frac{\partial N_1}{\partial z} & \frac{\partial N_1}{\partial y} & 0 & \frac{\partial N_2}{\partial z} & \frac{\partial N_2}{\partial y} & \mathsf{L} & 0 & \frac{\partial N_8}{\partial z} & \frac{\partial N_8}{\partial y} \end{bmatrix} \tag{3.15}$$

The displacement values at each node in directions *x*, *y* and *z* are solving from the finite element equation as given in Eq. (3.11). The hexahedron element can be considered as Fig. 3.2. The interpolation functions at each node are given by the following equation:

$$N_n = \frac{1}{8}(1+\xi_n\xi)(1+\eta_n\eta)(1+\zeta_n\zeta). \tag{3.16}$$

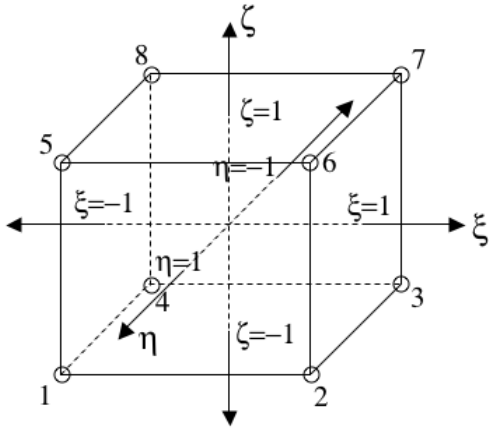

Figure 3.2: Hexahedron element and its local geometry

The matrix [*C*] for a hexahedron element is as follows:

$$[C]=\frac{E}{(1+\nu)(1-2\nu)}\begin{bmatrix}(1-\nu) & \nu & \nu & 0 & 0 & 0\\ & (1-\nu) & \nu & 0 & 0 & 0\\ & & (1-\nu) & 0 & 0 & 0\\ & & & \frac{(1-2\nu)}{2} & 0 & 0\\ SYM & & & & \frac{(1-2\nu)}{2} & 0\\ & & & & & \frac{(1-2\nu)}{2}\end{bmatrix} \tag{3.17}$$

where E is Young's Modulus and ν is Poisson's ratio. The stiffness matrix $[K^*]$ can be calculated by using Gauss-Legendre integration formula. Thus the $[K^*]$ matrix in Eq. (3.12) becomes:

$$\begin{aligned}[K^*] &= \int_{-1}^{1}\int_{-1}^{1}\int_{-1}^{1}[B(\xi,\eta,\zeta)]^T[C][B(\xi,\eta,\zeta)]|J|(\xi,\eta,\zeta)d\xi d\eta d\zeta \\ &\approx \sum_{i=1}^{NG}\sum_{j=1}^{NG}\sum_{k=1}^{NG}W_iW_jW_k[B(\xi,\eta,\zeta)]^T[C][B(\xi,\eta,\zeta)]|J|(\xi,\eta,\zeta)d\xi d\eta d\zeta\end{aligned} \tag{3.18}$$

where $|J|$ is the determinant of the Jacobian transformation between the global and local volume coordinates. W is the weight with the subscripts (i,j,k) and NG is the number of Gauss points. For the plane (x, y) problem, the stiffness matrix becomes

$$[K^*]=\int_S [B]^T[C][B]dS \tag{3.19}$$

$$\{F_B\}=\int_S [N]^T\{F\}dS \tag{3.20}$$

$$\{F_t\}=\int_x [N]^T\{T_y\}dx \text{ or } \int_y [N]^T\{T_x\}dy \tag{3.21}$$

The matrix [B] for a 4-node quadratic element is as follows:

$$[B]=\begin{bmatrix}\frac{\partial N_1}{\partial x} & 0 & \frac{\partial N_2}{\partial x} & 0 & \frac{\partial N_3}{\partial x} & 0 & \frac{\partial N_4}{\partial x} & 0\\ 0 & \frac{\partial N_1}{\partial y} & 0 & \frac{\partial N_2}{\partial y} & 0 & \frac{\partial N_3}{\partial y} & 0 & \frac{\partial N_4}{\partial y}\\ \frac{\partial N_1}{\partial y} & \frac{\partial N_1}{\partial x} & \frac{\partial N_2}{\partial y} & \frac{\partial N_2}{\partial x} & \frac{\partial N_3}{\partial y} & \frac{\partial N_3}{\partial x} & \frac{\partial N_4}{\partial y} & \frac{\partial N_4}{\partial x}\end{bmatrix}. \tag{3.22}$$

The 4-node quadratic element can be considered as Fig. 3.3. The interpolation functions at each node are given by:

$$N_n = \frac{1}{4}(1+\xi_n\xi)(1+\eta_n\eta). \tag{3.23}$$

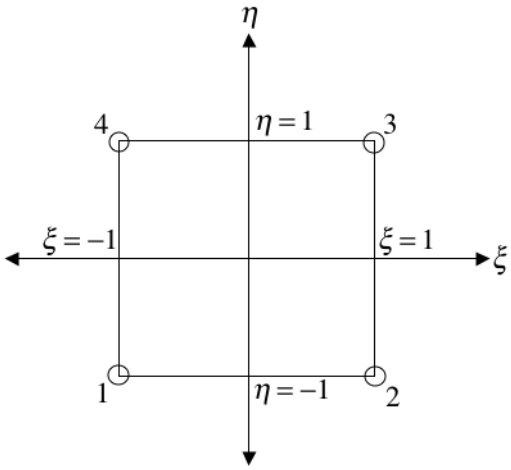

Figure 3.3 A 4-node quadratic element and its local geometry

The matrix [*C*] for plane stress case is

$$[C] = \frac{E}{1-\nu^2}\begin{bmatrix} 1 & \nu & 0 \\ & 1 & 0 \\ SYM & & \frac{1-\nu}{2} \end{bmatrix}. \tag{3.24}$$

The matrix [*C*] for plane strain case is

$$[C] = \frac{E}{1+\nu}\begin{bmatrix} \frac{1-\nu}{1-2\nu} & \frac{\nu}{1-2\nu} & 0 \\ & \frac{1-\nu}{1-2\nu} & 0 \\ SYM & & \frac{1}{2} \end{bmatrix}. \tag{3.25}$$

Finally, stress component is in the form of the following equation

$$\{\sigma\} = [C]\{\varepsilon\} \tag{3.26}$$

The stiffness matrix $[K^*]$ in Eq. (3.19) can be also calculated as the same as three-dimensional FEM by using Gauss-Legendre integration formula.

$$\begin{aligned}\left[K^*\right] &= \int_{-1}^{1}\int_{-1}^{1}\left[B(\xi,\eta)\right]^T[C]\left[B(\xi,\eta)\right]|J|(\xi,\eta)d\xi d\eta \\ &\approx \sum_{i=1}^{NG}\sum_{j=1}^{NG}W_iW_j\left[B(\xi,\eta)\right]^T[C]\left[B(\xi,\eta)\right]|J|(\xi,\eta)d\xi d\eta\end{aligned} \tag{3.27}$$

3.3 Plane Stress and Strain

The general state of stress at a point is characterized by six independent normal and shear stress component, which act on the faces of an element of material located at the point, Fig. 3.4. This state of stress, however, is not often encountered in the approximations or simplifications of the loading on a body in order that the stress produced in a structural member or mechanical element can be analyzed in a single plane. When this is the case, the material is said to be subjected to plane stress, Fig. 3.5. For example, if there is no load on the surface of a body, then the normal and shear stress components will be zero on the face of an element that lies on the surface. Consequently, the corresponding stress components on the opposite face will also be zero, and so the material at the point will be subjected to plane stress

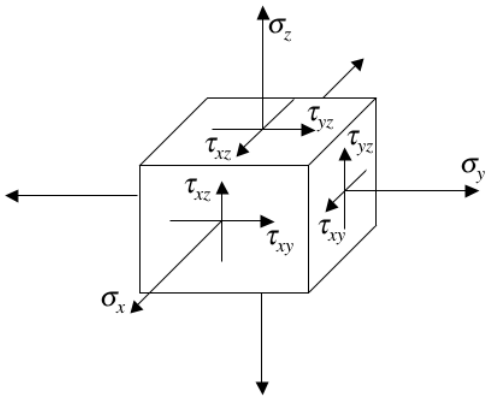

Figure 3.4: General state of stress for material

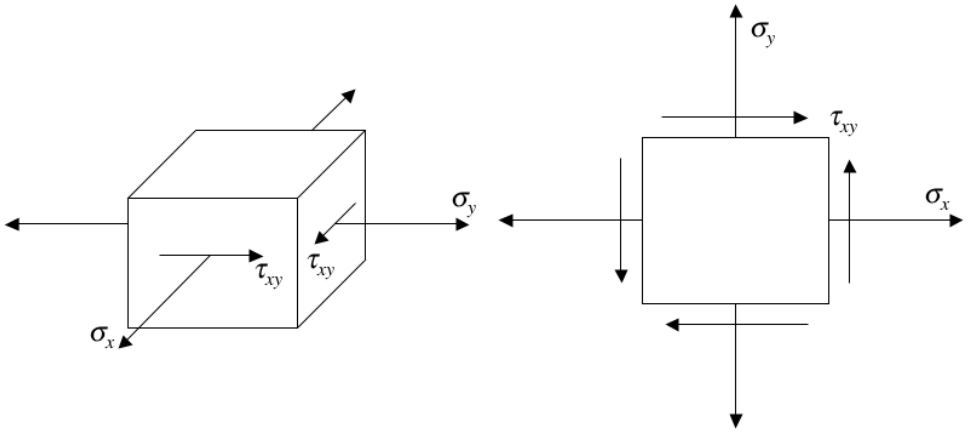

Figure 3.5: Plane stress in *x*-*y* coordinate system

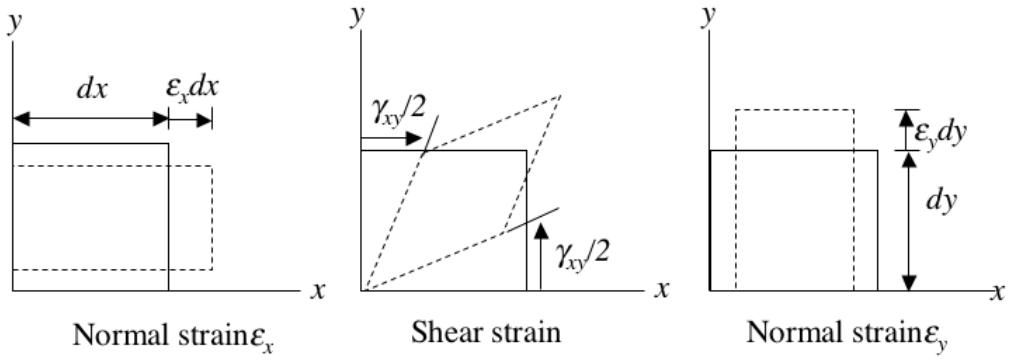

Figure 3.6: Plane Strain in *x*-*y* coordinate system

Like the plane stress, we will not consider the effects of the component ε_z, γ_{xz} and γ_{yz}. In general, then a plane-strained element is subjected to two components of normal strain, ε_x, ε_y, and one component of shear strain, γ_{xy}. The deformations of an element caused by each of these strains are shown graphically in Fig. 3.6. The normal strains are produced by changes in length of the element in the *x* and *y* directions, and the shear strain is produced by the relative rotation of two adjacent sides of the element.

3.4 Elasticity Theory of Material

Elasticity theory is formulated in terms of many different types of variables that are either specified or sought at spatial points in the body under study. Some of these variables are scalar quantities, representing a single magnitude at each point in space. Common examples include the material density ρ and material moduli such as Young's modulus *E*, Poisson's ratio ν, or the shear modulus μ. Other variables of interest are vector quantities that are expressible in terms of components in a two- or three-dimensional coordinate system. Examples of vector variables are the displacement and rotation of material points in the elastic continuum. Formulations within the theory also require the need for matrix variables, which commonly require more than three components to quantify. Examples of such variables include stress and strain. As shown in subsequent section, a three-dimensional formulation requires nine components (only six are independent) to quantify the stress or strain at a point. For this case, the variable is normally expressed in a matrix format with three rows and three columns. To summarize this discussion, in a three-dimensional Cartesian coordinate system, scalar, vector, and matrix variables can thus be written as follows:

Mass density scalar = ρ

Displacement vector $\boldsymbol{u} = u\boldsymbol{e_1} + v\boldsymbol{e_2} + w\boldsymbol{e_3}$

$$\text{Stress matrix} = [\sigma] = \begin{bmatrix} \sigma_x & \tau_{xy} & \tau_{xz} \\ \tau_{yx} & \sigma_y & \tau_{yz} \\ \tau_{zx} & \tau_{zy} & \sigma_z \end{bmatrix} \tag{3.28}$$

where $\boldsymbol{e_1}$, $\boldsymbol{e_2}$, $\boldsymbol{e_3}$ are the usual unit basis vectors in the coordinate directions. Thus, scalars, vectors, and matrices are specified by one, three, and nine components, respectively.

The formulation of elasticity problems not only involves these types of variables, but also incorporates additional quantities that require even more components to characterize. Because of this, most field theories such as elasticity make use of a tensor formalism using index notation. This enables efficient representation of all variables and governing equations using a single standardized scheme. The tensor concept is defined more precisely, but simply says that scalars, vectors, matrices, and other higher-order variables can all be represented by tensors of various orders.

3.5 Strain-displacement Relations

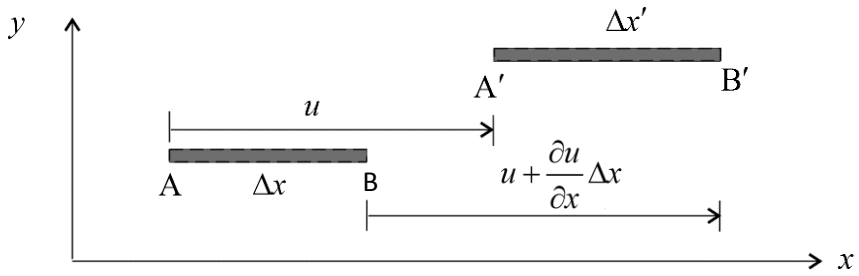

Figure 3.7: Displacement on the AB line segment

Let consider a Δx long segment that undergoes a change in length, the new length being denoted by $\Delta x'$. From Fig. 3.7 it is seen that [38].

$$u + \Delta x' = \Delta x + \left(u + \frac{\partial u}{\partial x} \Delta x \right) \tag{3.29}$$

Where u and $u + \frac{\partial u}{\partial x} \Delta x$ are the displacements of points A and B, respectively, in the x direction. Accordingly, the normal strain in the x direction is

$$\varepsilon_x = \frac{\Delta x' - \Delta x}{\Delta x} = \frac{\partial u}{\partial x} \tag{3.30}$$

Similarly, in the y and z directions the normal strains are:

$$\varepsilon_y = \frac{\partial v}{\partial y} \tag{3.31}$$

$$\varepsilon_z = \frac{\partial w}{\partial z} \tag{3.32}$$

Where v and w are the displacements in y and z directions, respectively.

For angular deformation the tensorial shear strain is the average change in the angle between two mutually perpendicular lines.

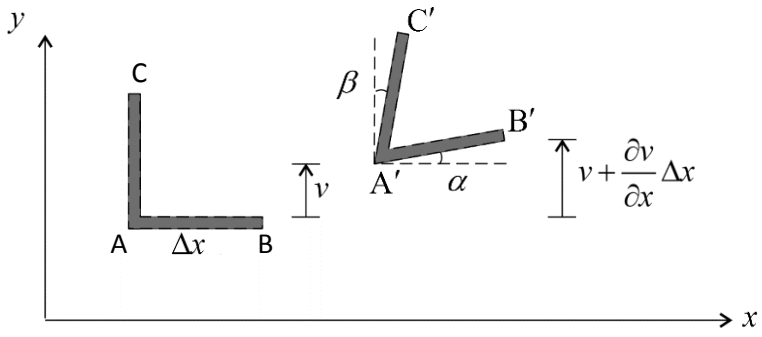

Figure 3.8: Displacement of the ABC segment

From Fig. 3.8,

$$\varepsilon_{xy} = \frac{\alpha + \beta}{2} \tag{3.33}$$

For small deformation

$$\alpha \approx \tan\alpha = \frac{\left(v + \frac{\partial v}{\partial x}\Delta x\right) - \mathrm{v}}{\Delta x} = \frac{\partial v}{\partial x} \tag{3.34}$$

Similarly $\beta = \frac{\partial u}{\partial y}$, and the xy component of the tensorial shear strain is

$$\varepsilon_{xy} = \frac{1}{2}\left(\frac{\partial u}{\partial y} + \frac{\partial v}{\partial x}\right) \tag{3.35}$$

In a similar manner, obtain the following expression for the ε_{yz} and ε_{xz} components of the tensorial shear strains:

$$\varepsilon_{yz} = \frac{1}{2}\left(\frac{\partial v}{\partial z} + \frac{\partial w}{\partial y}\right) \tag{3.36}$$

$$\varepsilon_{xz} = \frac{1}{2}\left(\frac{\partial u}{\partial z} + \frac{\partial w}{\partial x}\right) \tag{3.37}$$

The engineering shear strains are twice the tensorial shear strains:

$$\gamma_{yz} = 2\varepsilon_{yz} = \frac{\partial v}{\partial z} + \frac{\partial w}{\partial y} \tag{3.38}$$

$$\gamma_{xz} = 2\varepsilon_{xz} = \frac{\partial u}{\partial z} + \frac{\partial w}{\partial x} \tag{3.39}$$

$$\gamma_{xy} = 2\varepsilon_{xy} = \frac{\partial u}{\partial y} + \frac{\partial v}{\partial x} \tag{3.40}$$

Thus, in matrix form Eq. (3.30) to Eq. (3.32) and Eq. (3.38) to Eq. (3.40) can be written as,

$$\begin{Bmatrix} \varepsilon_x \\ \varepsilon_y \\ \varepsilon_z \\ \gamma_{xy} \\ \gamma_{yz} \\ \gamma_{zx} \end{Bmatrix} = \begin{bmatrix} \partial/\partial x & 0 & 0 \\ 0 & \partial/\partial y & 0 \\ 0 & 0 & \partial/\partial z \\ \partial/\partial y & \partial/\partial x & 0 \\ 0 & \partial/\partial z & \partial/\partial y \\ \partial/\partial z & 0 & \partial/\partial x \end{bmatrix} \begin{Bmatrix} u \\ v \\ w \end{Bmatrix} \tag{3.41}$$

Or

$$\{\varepsilon\} = [D]\{u\} \tag{3.42}$$

Where,

$$[D] = \begin{bmatrix} \partial/\partial x & 0 & 0 \\ 0 & \partial/\partial y & 0 \\ 0 & 0 & \partial/\partial z \\ \partial/\partial y & \partial/\partial x & 0 \\ 0 & \partial/\partial z & \partial/\partial y \\ \partial/\partial z & 0 & \partial/\partial x \end{bmatrix}$$

3.6 Equilibrium Equations

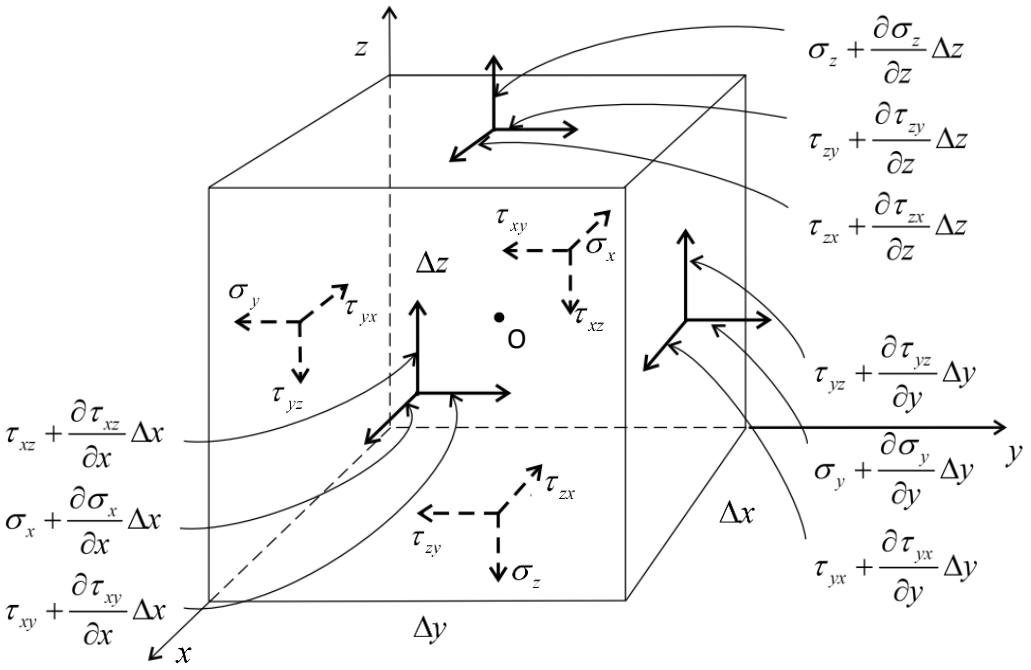

Figure 3.9: Stresses on the $\Delta x \Delta y \Delta z$ cubic element

The equilibrium equations at a point O are obtained by considering force and moment balances on a small $\Delta x \Delta y \Delta z$ cubic element located at point O, Fig, 3.9. It relates the stresses at one face to those at the opposite face by the Taylor series. By using only the first term of the Taylor series, force balance in the x direction gives [38].

$$\begin{aligned} &-\sigma_x \Delta z \Delta y - \tau_{zx} \Delta x \Delta y - \tau_{yx} \Delta x \Delta z + \left(\sigma_x + \frac{\partial \sigma_x}{\partial x} \Delta x \right) \Delta z \Delta y \\ &+ \left(\tau_{zx} + \frac{\partial \tau_{zx}}{\partial z} \Delta z \right) \Delta x \Delta y + \left(\tau_{yx} + \frac{\partial \tau_{yx}}{\partial y} \Delta y \right) \Delta x \Delta z + b_x \Delta x \Delta y \Delta z = 0 \end{aligned} \tag{3.43}$$

Where b_x is the body force per unit volume in the x-direction. After simplification, this equation becomes

$$\frac{\partial \sigma_x}{\partial x} + \frac{\partial \tau_{yx}}{\partial y} + \frac{\partial \tau_{zx}}{\partial z} + b_x = 0 \tag{3.44}$$

By similar arguments, the equilibrium equations in the y and z directions are

$$\frac{\partial \tau_{xy}}{\partial x} + \frac{\partial \sigma_y}{\partial y} + \frac{\partial \tau_{zy}}{\partial z} + b_y = 0 \tag{3.45}$$

$$\frac{\partial \tau_{xz}}{\partial x} + \frac{\partial \tau_{yz}}{\partial y} + \frac{\partial \sigma_z}{\partial z} + b_z = 0 \tag{3.46}$$

Where b_y and b_z are the body forces per unit volume in y and z directions.

Eq. (3.44) to Eq. (3.46) can be written as

$$\frac{\partial \sigma_{ij}}{\partial x_j} + b_i = 0 \tag{3.47}$$

A moment balance about an axis parallel to x and passing through the center gives [38]

$$\begin{aligned} &\tau_{yz}\Delta x\Delta z\frac{\Delta y}{2} - \tau_{zy}\Delta x\Delta y\frac{\Delta z}{2} + \left(\tau_{yz} + \frac{\partial \tau_{yz}}{\partial y}\Delta y\right)\Delta x\Delta z\frac{\Delta y}{2} \\ &\quad - \left(\tau_{zy} + \frac{\partial \tau_{zy}}{\partial z}\Delta z\right)\Delta x\Delta y\frac{\Delta z}{2} = 0 \end{aligned} \tag{3.48}$$

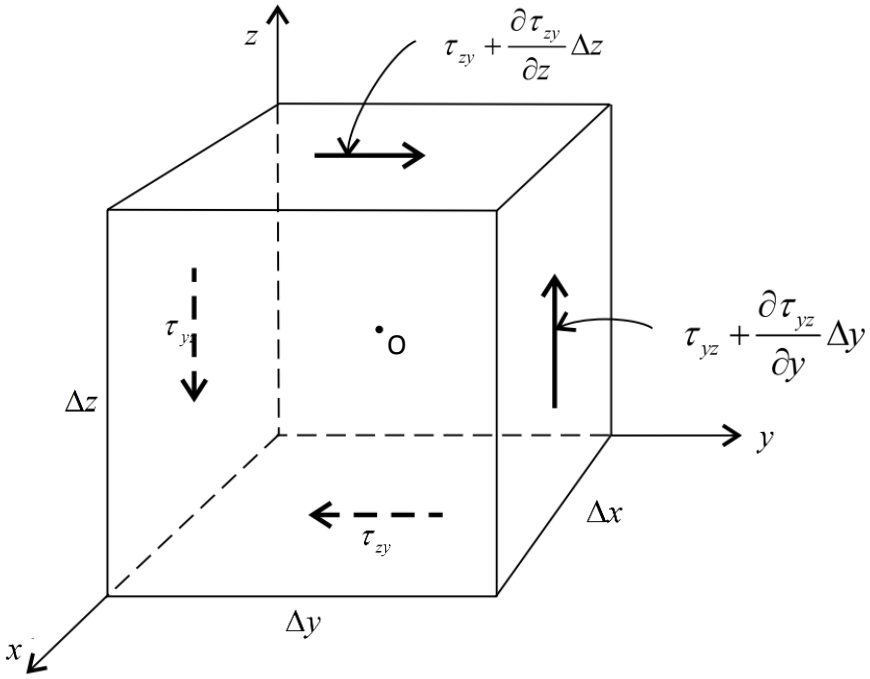

Figure 3.10: Stresses on the $\Delta x\Delta y\Delta z$ cubic element that appear in the moment balance about an axis parallel to x and passing through the center (Point O)

By omitting higher order terms, which vanish in the limit $\Delta x \to 0,\ \Delta y \to 0,\ \Delta z \to 0,$ this equation becomes

$$\tau_{yz} = \tau_{zy} \tag{3.49}$$

Similarly, we obtain the following equalities:

$$\tau_{xz} = \tau_{zx} \tag{3.50}$$

$$\tau_{xy} = \tau_{yx} \tag{3.51}$$

By virtue of Eqs. (3.49), (3.50) and (3.50) the three equilibrium equations, Eqs. (3.44), (3.45), and (3.46) contains six unknowns, namely, the three normal stresses $(\sigma_x, \sigma_y, \sigma_z)$ and the three shear stresses $(\tau_{yz}, \tau_{xz}, \tau_{xy})$.

3.7 Solution of Governing Equation

In finite element method, any three dimensional body is discretized into some finite solid element of simple geometric shape. There are various types of solid element used in finite element method. Amongst them the most simple is the tetrahedral element of four nodes. For linear problem 4-node tetrahedron, 5-node pyramid, 6-noded prism or 8-node brick elements can be used. Amongst them the 8-node brick element provides more accuracy. For the solution of quadratic equation higher order element are used. Some typical three dimensional solid elements are shown in Figs (3.11), (3.12), and (3.13).

Tetrahedron (Tet):

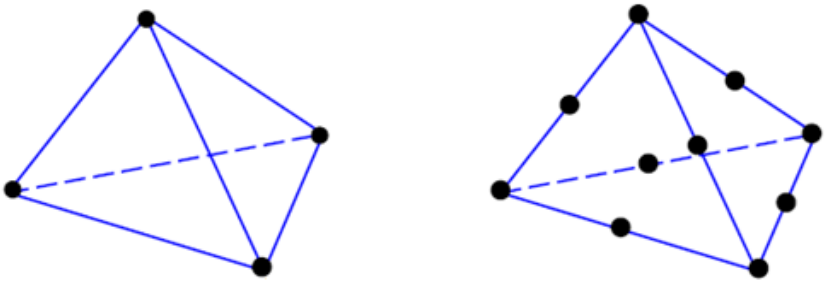

Linear (4 nodes) Quadratic (10 nodes)

Figure 3.11: Three dimensional Tetrahedron solid elements

Hexahedron (Brick):

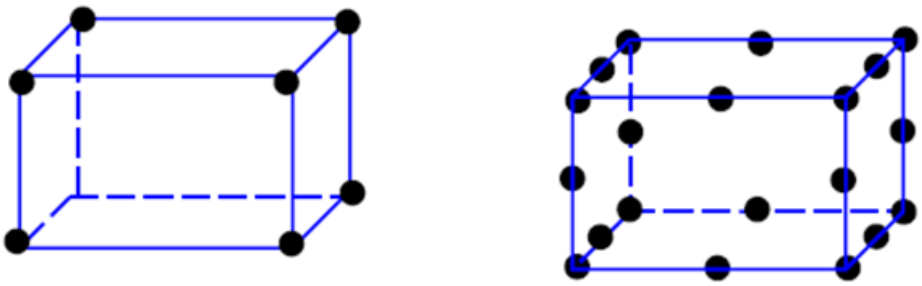

Linear (8 nodes) Quadratic (20 nodes)

Figure 3.12: Three dimensional Hexahedron solid elements

Prism:

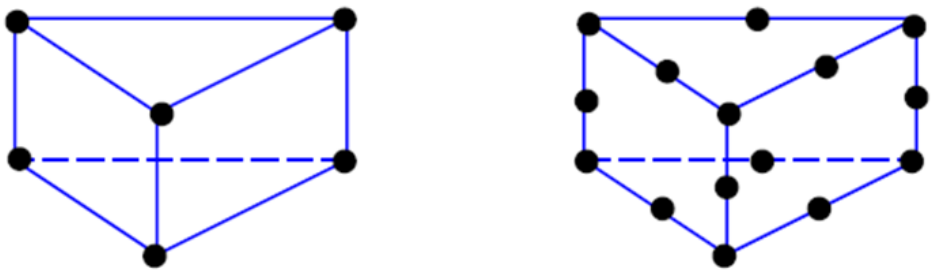

Linear (6 nodes) Quadratic (15 nodes)

Figure 3.13: Three dimensional prism solid elements

3.7.1 Isoparametric mapping

To represent an irregular shaped body, we must consider the elements of arbitrary shapes. But if the elements are distorted other than of regular shape then the determination of shape function and carrying out integration is very difficult. To ease integration in evaluating the virtual work, the isoparametric solid elements are considered. The term "isoparametric" means that geometry and displacement field is specified in parametric form and are interpolated with the same functions. Shape functions used for interpolation are polynomials of the local coordinates ξ, η and ζ $(-1 \le \xi, \eta, \zeta \le 1)$. Both coordinates and displacements are interpolated with the same shape functions and then the coordinates are mapped into the global coordinates.

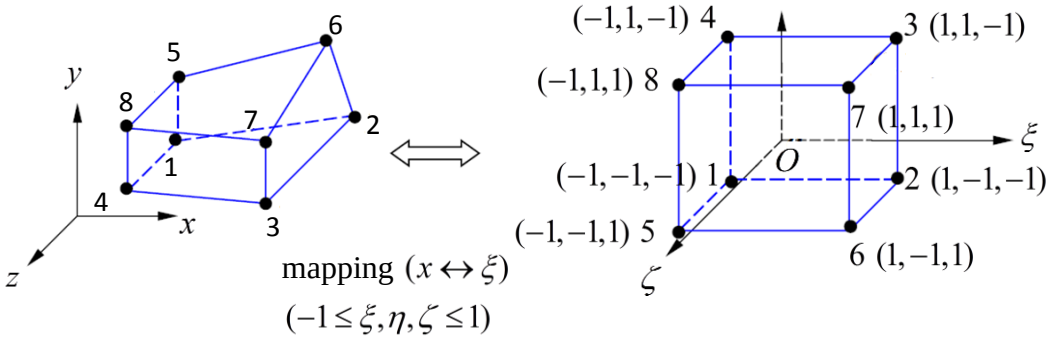

Figure 3.14: Transformation from local coordinate to global coordinate

Now, consider a linear 8-node hexahedron element in the global coordinate system (x, y, z) . The following function maps a point in the local coordinate system (ξ, η, ζ) to a point in global coordinate system:

$$x = \sum_{i=1}^{N} N_i x_i, \quad y = \sum_{i=1}^{N} N_i y_i, \quad z = \sum_{i=1}^{N} N_i z_i \tag{3.52}$$

The functions are linear combinations of the nodal coordinates. The coefficients N_1, N_2, N_3, N_4 are functions of ξ, η and ζ . They are the shape functions, so constructed that the eight corners of the hexahedron on the local coordinate system (ξ, η, ζ) to the eight nodes of the hexahedron on the global coordinate system (ξ, η, ζ).

The shape functions are given by

$$
\begin{aligned}
N_1(\xi,\eta,\zeta) &= \frac{1}{8}(1-\xi)(1-\eta)(1-\zeta), \quad & N_2(\xi,\eta,\zeta) &= \frac{1}{8}(1+\xi)(1-\eta)(1-\zeta),\\
N_3(\xi,\eta,\zeta) &= \frac{1}{8}(1+\xi)(1+\eta)(1-\zeta), \quad & N_4(\xi,\eta,\zeta) &= \frac{1}{8}(1-\xi)(1+\eta)(1-\zeta),\\
N_5(\xi,\eta,\zeta) &= \frac{1}{8}(1-\xi)(1-\eta)(1+\zeta), \quad & N_6(\xi,\eta,\zeta) &= \frac{1}{8}(1+\xi)(1-\eta)(1+\zeta),\\
N_7(\xi,\eta,\zeta) &= \frac{1}{8}(1+\xi)(1+\eta)(1+\zeta), \quad & N_8(\xi,\eta,\zeta) &= \frac{1}{8}(1-\xi)(1+\eta)(1+\zeta)
\end{aligned}
\tag{3.53}
$$

3.7.2 Interpolation of displacement

The displacement field is obtained by

$$u = \sum_{i=1}^{N} N_i u_i, \quad v = \sum_{i=1}^{N} N_i v_i, \quad w = \sum_{i=1}^{N} N_i w_i \tag{3.54}$$

In the matrix form, the displacement vector at a point in the element is an interpolation of the nodal displacements:

$$u = Nq \tag{3.55}$$

Where,

$$u = \{u, v, w\}^{\mathrm{T}}$$

$$q = \{u_1, v_1, w_1, u_2, v_2, w_2, ..., u_8, v_8, w_8\}^{\mathrm{T}} \text{ and,}$$

$$N = \begin{bmatrix} N_1 & 0 & 0 & N_2 & 0 & 0 & N_3 & 0 & 0 & ... & N_n & 0 & 0 \\ 0 & N_1 & 0 & 0 & N_2 & 0 & 0 & N_3 & 0 & ... & 0 & N_n & 0 \\ 0 & 0 & N_1 & 0 & 0 & N_2 & 0 & 0 & N_3 & ... & 0 & 0 & N_n \end{bmatrix}$$

Let the virtual nodal displacements be δq, the virtual displacement field in the elements is

$$\delta u = N \delta q \tag{3.56}$$

3.7.3 Expression of strains in terms of nodal displacements

From previous section it is known that,

$$\varepsilon = Du \tag{3.57}$$

Now using Eq. (3.55)

$$
\begin{aligned}
\varepsilon &= DNq \\
&= \begin{bmatrix} \partial/\partial x & 0 & 0 \\ 0 & \partial/\partial y & 0 \\ 0 & 0 & \partial/\partial z \\ \partial/\partial y & \partial/\partial x & 0 \\ 0 & \partial/\partial z & \partial/\partial y \\ \partial/\partial z & 0 & \partial/\partial x \end{bmatrix}
\begin{bmatrix} N_1 & 0 & 0 & N_2 & 0 & 0 & N_3 & 0 & 0 & ... & N_n & 0 & 0 \\ 0 & N_1 & 0 & 0 & N_2 & 0 & 0 & N_3 & 0 & ... & 0 & N_n & 0 \\ 0 & 0 & N_1 & 0 & 0 & N_2 & 0 & 0 & N_3 & ... & 0 & 0 & N_n \end{bmatrix} \{q\}
\end{aligned}
\tag{3.58}
$$

Or

$$\begin{aligned}\varepsilon &= \begin{bmatrix} B_1 & B_2 & B_3 & \dots & B_n \end{bmatrix} q \\ &= Bq \end{aligned} \tag{3.69}$$

Where,

$$B_i = \begin{bmatrix} \partial N_i/\partial x & 0 & 0 \\ 0 & \partial N_i/\partial y & 0 \\ 0 & 0 & \partial N_i/\partial z \\ \partial N_i/\partial y & \partial N_i/\partial x & 0 \\ 0 & \partial N_i/\partial z & \partial N_i/\partial y \\ \partial N_i/\partial z & 0 & \partial N_i/\partial x \end{bmatrix}$$

This $B = DN$ is called the strain-displacement matrix. N_i is expressed in the function of local coordinate (ξ, η, ζ) system. In order to calculate B matrix we need to convert the gradient on the (ξ, η, ζ) to that on the (x, y, z) system. Using the chain rule of differentiation, it is obtained that

$$\begin{aligned} \frac{\partial N_i}{\partial x} &= \frac{\partial N_i}{\partial \xi}\frac{\partial \xi}{\partial x} + \frac{\partial N_i}{\partial \eta}\frac{\partial \eta}{\partial x} + \frac{\partial N_i}{\partial \zeta}\frac{\partial \zeta}{\partial x} \\ \frac{\partial N_i}{\partial y} &= \frac{\partial N_i}{\partial \xi}\frac{\partial \xi}{\partial y} + \frac{\partial N_i}{\partial \eta}\frac{\partial \eta}{\partial y} + \frac{\partial N_i}{\partial \zeta}\frac{\partial \zeta}{\partial y} \\ \frac{\partial N_i}{\partial z} &= \frac{\partial N_i}{\partial \xi}\frac{\partial \xi}{\partial z} + \frac{\partial N_i}{\partial \eta}\frac{\partial \eta}{\partial z} + \frac{\partial N_i}{\partial \zeta}\frac{\partial \zeta}{\partial z} \end{aligned} \tag{3.60}$$

In matrix form

$$\begin{bmatrix} \frac{\partial N_i}{\partial x} \\ \frac{\partial N_i}{\partial y} \\ \frac{\partial N_i}{\partial z} \end{bmatrix} = \begin{bmatrix} \frac{\partial \xi}{\partial x} & \frac{\partial \eta}{\partial x} & \frac{\partial \zeta}{\partial x} \\ \frac{\partial \xi}{\partial y} & \frac{\partial \eta}{\partial y} & \frac{\partial \zeta}{\partial y} \\ \frac{\partial \xi}{\partial z} & \frac{\partial \eta}{\partial z} & \frac{\partial \zeta}{\partial z} \end{bmatrix} \begin{bmatrix} \frac{\partial N_i}{\partial \xi} \\ \frac{\partial N_i}{\partial \eta} \\ \frac{\partial N_i}{\partial \zeta} \end{bmatrix} \tag{3.61}$$

The 3×3 matrix that appears in Eq. (3.61) is called J^{-1} matrix which is obtained from the inverse of

$$J = \frac{\partial(x, y, z)}{\partial(\xi, \eta, \zeta)} = \begin{bmatrix} \frac{\partial x}{\partial \xi} & \frac{\partial y}{\partial \xi} & \frac{\partial z}{\partial \xi} \\ \frac{\partial x}{\partial \eta} & \frac{\partial y}{\partial \eta} & \frac{\partial z}{\partial \eta} \\ \frac{\partial x}{\partial \zeta} & \frac{\partial y}{\partial \zeta} & \frac{\partial z}{\partial \zeta} \end{bmatrix} \tag{3.62}$$

Matrix J is called the Jacobian matrix of (x,y,z) with respect to (ξ,η,ζ). In the finite element literature, matrices J and J^{-1} are called simply the Jacobian and Inverse Jacobian respectively. The notations are

$$J=\frac{\partial(x,y,z)}{\partial(\xi,\eta,\zeta)} \text{ and } J^{-1}=\frac{\partial(\xi,\eta,\zeta)}{\partial(x,y,z)}$$

The Jacobian matrix for any element is computed by differentiating the Eq. (3.54) for that element. Differentiating Eq. (3.54)

$$J=\begin{bmatrix} x_i\frac{\partial N_i}{\partial\xi} & y_i\frac{\partial N_i}{\partial\xi} & z_i\frac{\partial N_i}{\partial\xi} \\ x_i\frac{\partial N_i}{\partial\eta} & y_i\frac{\partial N_i}{\partial\eta} & z_i\frac{\partial N_i}{\partial\eta} \\ x_i\frac{\partial N_i}{\partial\zeta} & y_i\frac{\partial N_i}{\partial\zeta} & z_i\frac{\partial N_i}{\partial\zeta} \end{bmatrix}=\begin{bmatrix} J_{11} & J_{12} & J_{13} \\ J_{21} & J_{22} & J_{23} \\ J_{31} & J_{32} & J_{33} \end{bmatrix} \tag{3.63}$$

Then J^{-1} becomes

$$J^{-1}=\frac{1}{|J|}\begin{bmatrix} J_{11}' & J_{12}' & J_{13}' \\ J_{21}' & J_{22}' & J_{23}' \\ J_{31}' & J_{32}' & J_{33}' \end{bmatrix} \tag{3.64}$$

Where,

$$\begin{aligned} J_{11}' &= J_{22}J_{33}-J_{23}J_{32}, & J_{22}' &= J_{33}J_{11}-J_{31}J_{13} \\ J_{33}' &= J_{11}J_{22}-J_{12}J_{21}, & J_{12}' &= J_{23}J_{31}-J_{21}J_{33} \\ J_{23}' &= J_{31}J_{12}-J_{32}J_{11}, & J_{31}' &= J_{12}J_{23}-J_{13}J_{22} \\ J_{21}' &= J_{32}J_{13}-J_{12}J_{33}, & J_{32}' &= J_{13}J_{21}-J_{23}J_{11} \\ J_{13}' &= J_{21}J_{32}-J_{31}J_{22}, & |J| &= J_{11}J_{11}'+J_{12}J_{21}'+J_{13}J_{31}' \end{aligned} \tag{3.65}$$

The transformation of integrals from the global coordinate system to the local coordinate system is performed by the determinant of the Jacobian matrix:

$$dV=dxdydz=|J|\,d\xi d\eta d\zeta \tag{3.66}$$

Then from Eq. (3.61) becomes,

$$\begin{bmatrix} \frac{\partial N_i}{\partial x} \\ \frac{\partial N_i}{\partial y} \\ \frac{\partial N_i}{\partial z} \end{bmatrix}=\frac{1}{|J|}\begin{bmatrix} J_{11}' & J_{12}' & J_{13}' \\ J_{21}' & J_{22}' & J_{23}' \\ J_{31}' & J_{32}' & J_{33}' \end{bmatrix}\begin{bmatrix} \frac{\partial N_i}{\partial\xi} \\ \frac{\partial N_i}{\partial\eta} \\ \frac{\partial N_i}{\partial\zeta} \end{bmatrix} \tag{3.67}$$

From Eq. (3.67) the values of the derivative is readily obtained. Thus the B matrix is also obtained.

3.7.4 Expression of stress field in terms of the nodal displacements

It is known that

$$\sigma = C\varepsilon$$

Putting $\varepsilon = Bq$ in this equation

$$\sigma = CBq \tag{3.68}$$

From principle of virtual work it is known that,

$$\int_V \delta u^T b dV + \int_S \delta u^T t dS = \int_V \delta\varepsilon^T \sigma dV \tag{3.69}$$

Now putting $\delta u = N\delta q$, $\delta\varepsilon = B\delta u = BN\delta q$ and $\sigma = C\varepsilon = CBq$ in Eq. (3.69)

$$\int_V (N\delta q)^T b dV + \int_S (N\delta q)^T t dS = \int_V (B\delta q)^T CBq dV$$

$$\Rightarrow \int_V N^T \delta q^T b dV + \int_S N^T \delta q^T t dS = \int_V B^T \delta q^T CBq dV$$

$$\Rightarrow \int_V N^T b dV + \int_S N^T t dS = \int_V B^T CBq dV \tag{3.70}$$

In this equation $\int_V N^T b dV$ is the body force which acts over the total volume of the element and $\int_S N^T t dS$ is the applied surface traction. Thus the equation can be written as

$$Kq = f \tag{3.71}$$

Where, $f = \int_V N^T b dV + \int_S N^T t dS$ represents the total force acting on the element and K is the stiffness matrix which is given by

$$K = \int_V B^T CB dV \tag{3.72}$$

Putting $dV = dxdydz = |J| d\xi d\eta d\zeta$

$$K = \int_{-1}^{1}\int_{-1}^{1}\int_{-1}^{1} B^T CB |J| d\xi d\eta d\zeta \tag{3.73}$$

To evaluate the stiffness matrix K, the numerical integration formula over Gauss quadrature is applied. If any integral of the following form

$$I = \int_{-1}^{1} f(\xi) d\xi \tag{3.74}$$

Then to evaluate this integral a set of n points $\xi_1, \xi_2, \xi_3, ..., \xi_n$ is selected in the interval $(-1,1)$. The function is evaluated at these points *i.e.* $f(\xi_1), f(\xi_2), f(\xi_3), ..., f(\xi_n)$. Then the integral is a linear combination of these functional values

$$I = \int_{-1}^{1} f(\xi)\, d\xi = w_1 f(\xi_1) + w_2 f(\xi_2) + ... + w_n f(\xi_n) = \sum_{i=1}^{n} w_i f(\xi_i) \tag{3.75}$$

Thus it can be written as

$$K = \sum_{i=1}^{p_1} \sum_{j=1}^{p_2} \sum_{k=1}^{p_3} w_1 w_2 w_3 B_{ijk}{}^T C B_{ijk} \left| J_{ijk} \right| \tag{3.76}$$

Here p_1, p_2 and p_3 are the numbers of Gauss points in the ξ, η and ζ direction, respectively, while B_{ijk} and $\left|J_{ijk}\right|$ are abbreviations for

$$B_{ijk} \equiv B(\xi_i, \eta_j, \zeta_k), \left|J_{ijk}\right| = \det J(\xi_i, \eta_j, \zeta_k)$$

Usually the number of integration points is taken same in all directions *i.e.* $p = p_1 = p_2 = p_3$. The total number of Gauss points is thus p^3. Each point adds at most 6 to the stiffness matrix rank. For the 8-node hexahedron this rules gives $p = 2$.

CHAPTER IV

Analysis Model and Result Verification

4.1 Model for Analysis

The model considered for the analysis is shown in Fig. 4.1 can be used as a standard numerical model to investigate the characteristics of stress field and compare the numerical results with other methods. In the present study, the three-dimensional dissimilar material joint is subjected by a uniform tensile stress 1 MPa. The joint structure is symmetrical in x =10 mm and y =10 mm planes. The FEM model and boundary conditions are shown in Fig. 4.2. The small elements are arranged near the corner and alone the edge.

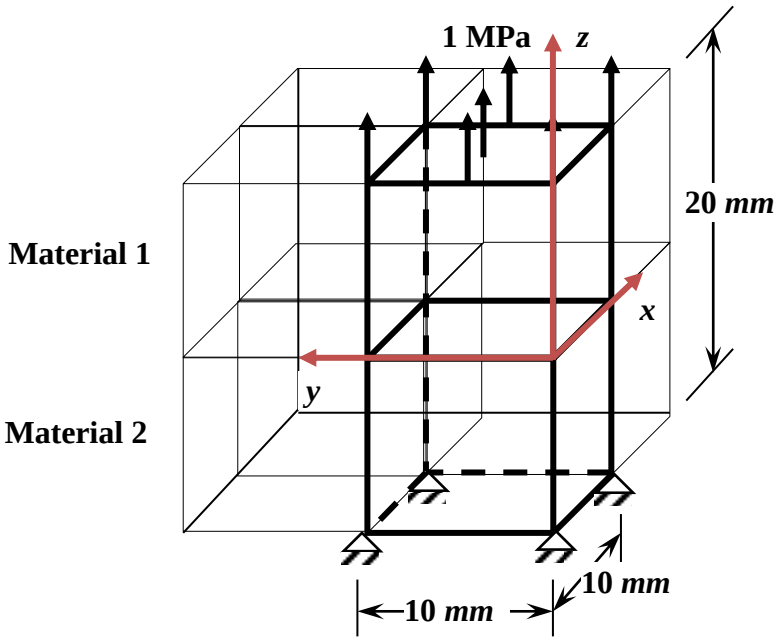

Figure 4.1: Model of anisotropic bonded joint

A uniform tensile stress is applied on upper side of FEM model in the z-direction. The FEM model is fixed in the x-direction on the right side, fixed in the y-direction on the back and fixed in the z-direction at the bottom of the model. For the symmetric nature one fourth of the model is considered for the analysis. The dimensions of the model are taken $10 \times 10 \times 20$ mm in the x, y and z direction respectively.

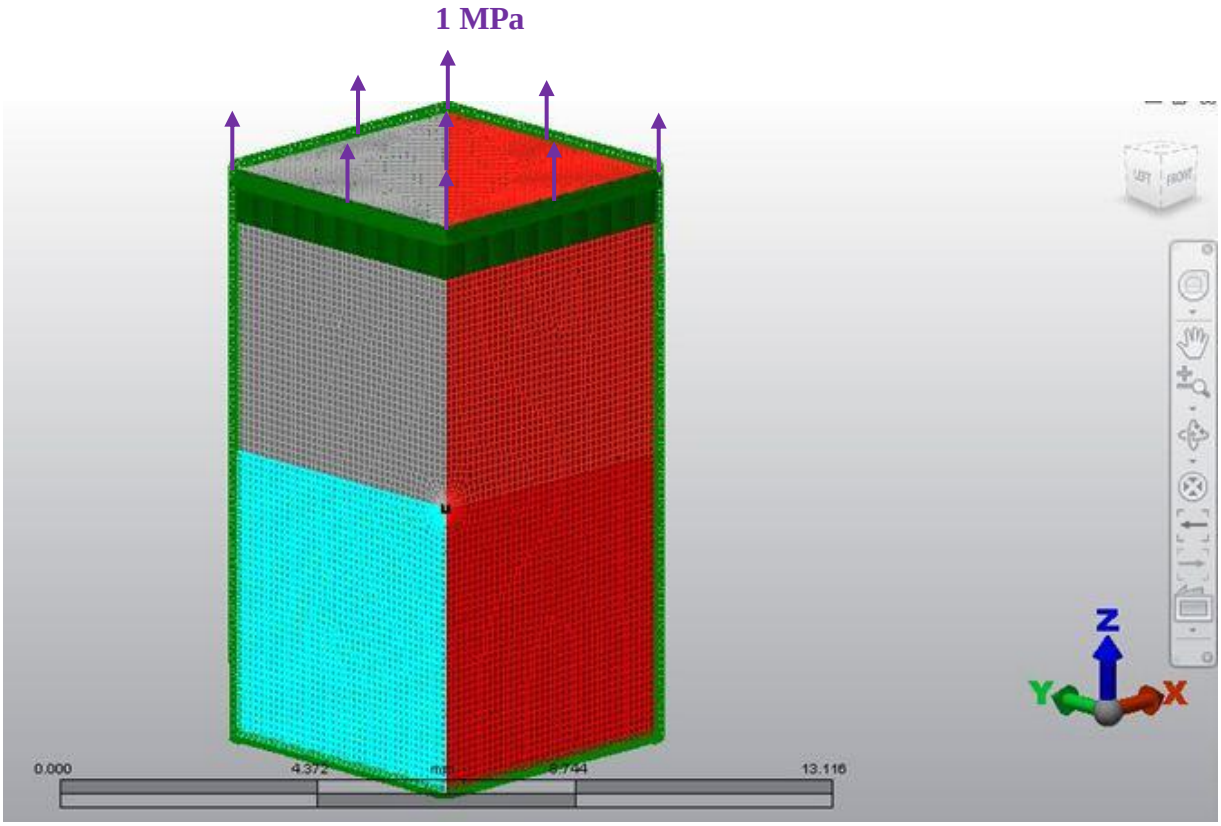

Figure 4.2: FEM model and boundary connections

4.2 Material Properties

The material properties of upper and lower material in dissimilar anisotropic elastic joint are shown in Table 4.1. The upper material (material 1) is hard and the lower material (material 2) is soft. The upper and lower materials used in present analysis are Silicon and Resin.

Table 4.1 Material properties for anisotropic materials

Material	Young's modulus (GPa)	Poisson's Ratio, ν
Silicon	166	0.26
2	2.74	0.38

4.3 Generation of Mesh Model

The mesh of the present model shown in Fig. 4.2 was generated by the finite element code Autodesk Simulation Mechanical 2015. Fixed boundary condition is applied in the bottom surface. Symmetric boundary condition was applied in the two inner surface along x and y direction. A distributed load of 1 MPa was applied on the top surface along positive z direction. The mesh applied was a mixture of tetrahedron, pyramid, wedge and hexahedron.

Overall mesh size was 0.5 mm whereas; at the vicinity of the vertex the mesh was refined to 0.0004035 mm. The total number of solid element was 520735. The mesh used at the interface corner of the analysis is shown in Fig. 4.3.

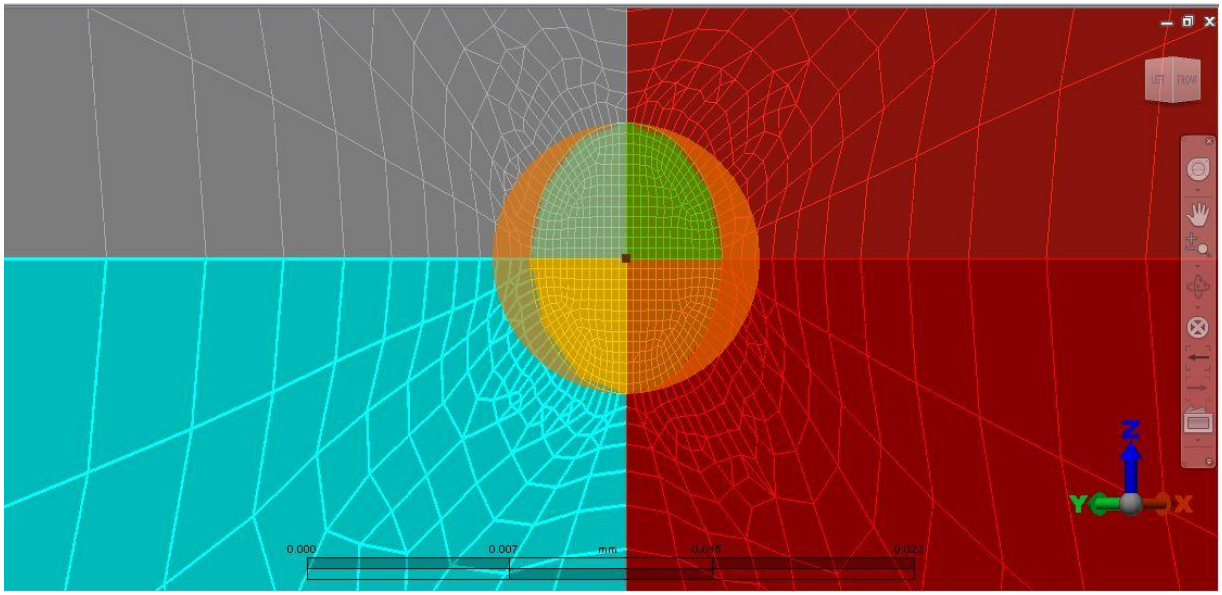

Figure 4.3: Mesh Model near the vertex of joint

After the discretization, the numerical calculations were carried out through finite element method by using Autodesk Simulation Mechanical 2015. The displacement, strain tensors and stress tensors were calculated in both rectangular and spherical coordinate system.

4.4 Accuracy Verification of Present Analysis

In order to check the accuracy of finite element method the bi-material joint of Silicon and Resin having slanted side surface which was analyzed by Koguchi and Costa [39] in boundary element method, BEM has been analyzed again with the present method applying the same boundary condition. The obtained results have been compared with that obtained by Koguchi. The graph is given below.

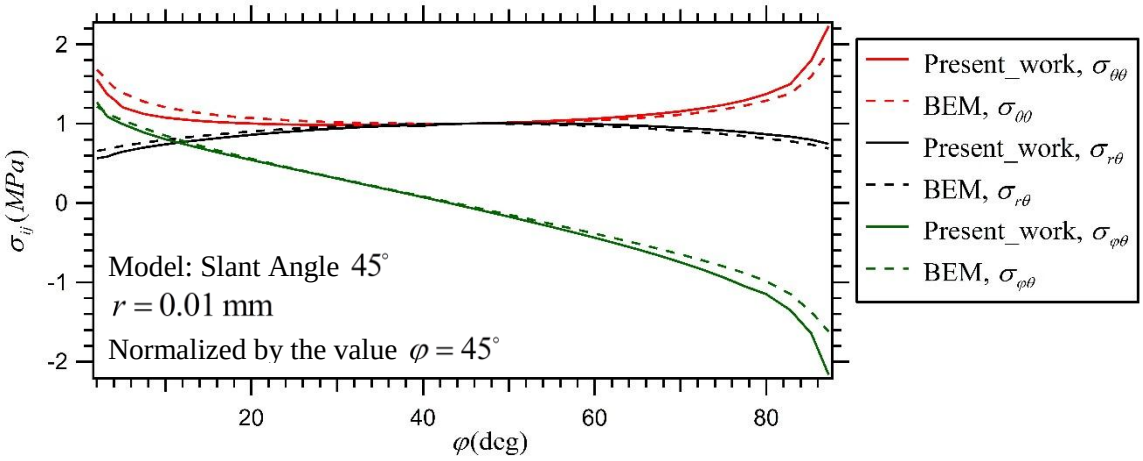

Figure 4.4: Comparison of normalized stress distribution obtained by FEM and BEM

From the graph it has been seen that the results obtained by present method is very near the result obtained by BEM. Thus the accuracy of the finite element method is verified. The accuracy of Autodesk Simulation Mechanical 2015 software is check by comparing the result with the bi-material joint of carbon/epoxy prepreg (SEAL Texipreg CC206 – T300 twill 2_2 fabric/toughened ET442 resin) and bonded with a 3M 9323 B/A epoxy adhesive, which was analyzed by Michele, Paolo and Marino by Ansys_Version 13 software package [40]. The graph is given below. From the graph it has been seen that the results obtained by Autodesk Simulation Mechanical 2015 is very near the results obtained by Ansys_version 13 software package. The maximum variation of result is about 2.25%.

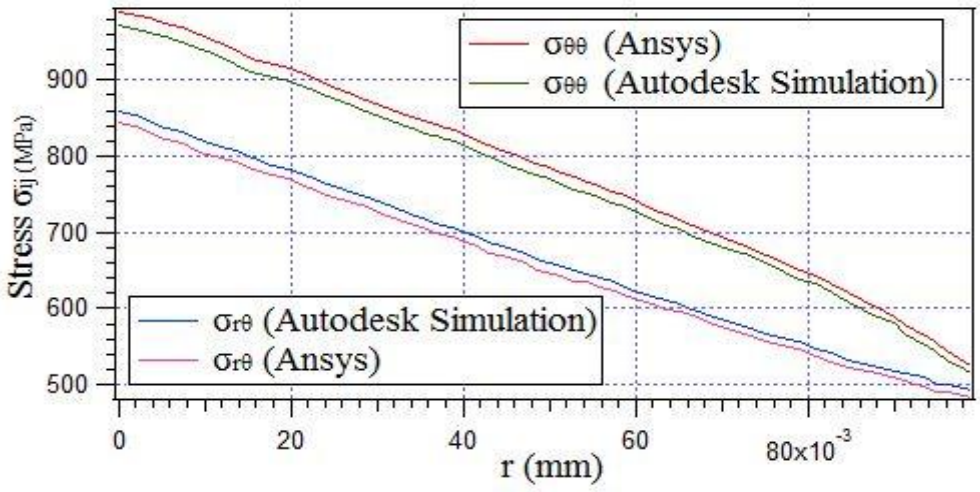

Figure 4.5: Comparison of result between Ansys and Autodesk Simulation

CHAPTER V

Result and Discussions

5.1 Numerical Result

In this study, Autodesk Simulation Mechanical 2015 student version software was used to analyze the stress field around the vertex in anisotropic dissimilar material joints. The FEM is a numerical method for finding approximate solutions of partial differential equations in physical problems under their boundary conditions. The physical problems are divided into many elements connecting by nodes. The approximate solutions are formed in each element and then assembled to be a main equation. Finally, the unknown parameters at nodes are known by solving the main equation.

5.1.1 Distribution of Elastic displacement

The variations of displacement fields on the r - ϕ plane in spherical coordinates are shown in Figs. 5.1 to 5.3. Figure shows the distribution of nodal elastic displacement of 3D anisotropic elastic bonded joint of silicon and resin. All of these graph show that the displacement is continuous at the interface. The interface of the joint is at $\theta = 90^{o}$.

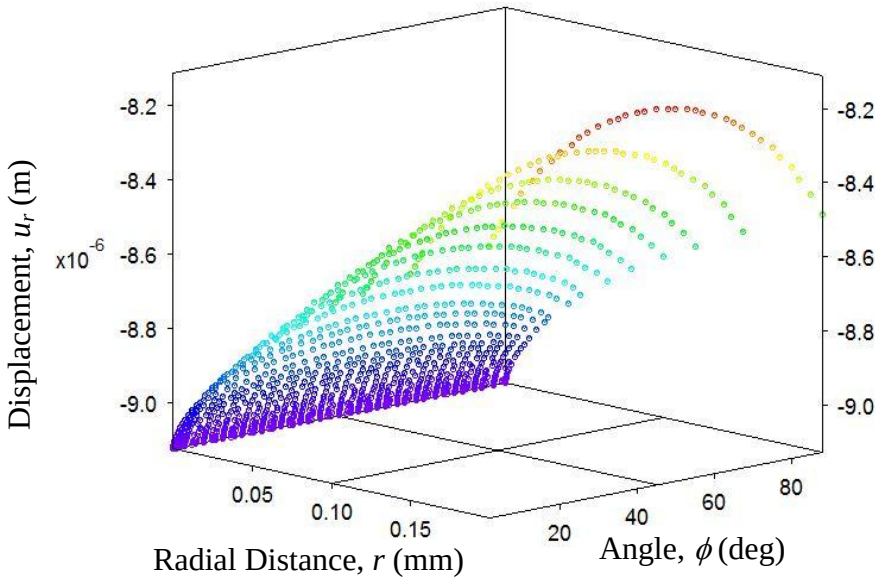

Figure 5.1: Distribution of nodal elastic displacement, u_r against r and ϕ at interface

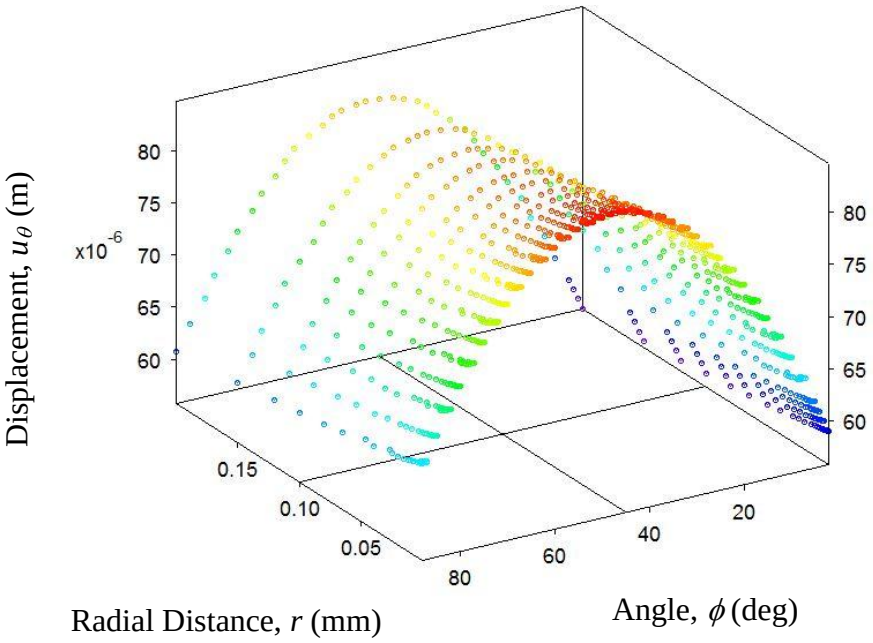

Figure 5.2: Distribution of nodal elastic displacement, u_θ against r and ϕ at interface

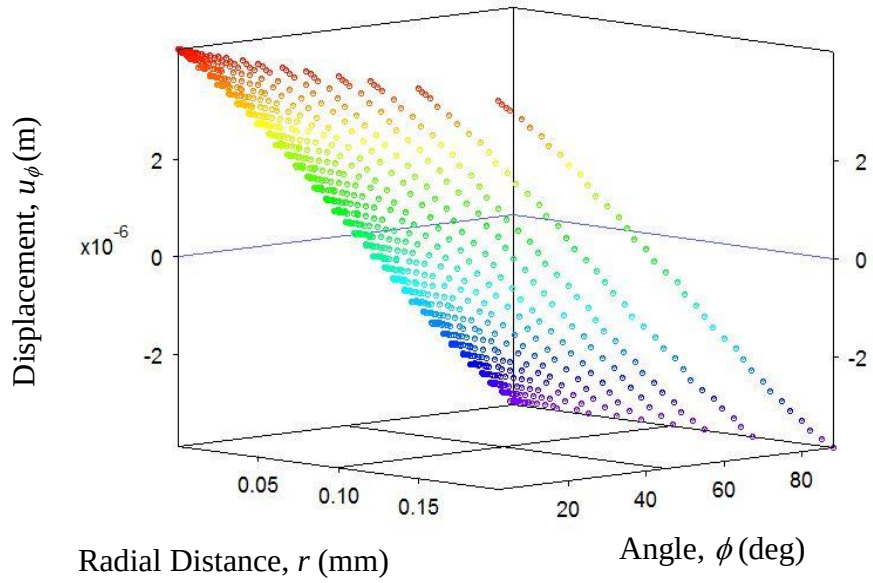

Figure 5.3: Distribution of nodal elastic displacement, u_ϕ against r and ϕ at interface

From the figure, it is found that, the elastic displacement is continuous at the interface of the joint and had higher value at the free edge than the inner portion. So there is a possibility to debond the joint near the free edge of the joint. It is also found that the elastic displacement at $\phi = 0°$ is agreed with that at $\phi = 90°$. The u_θ and u_r graph is symmetry with respect to angle, ϕ and u_ϕ is anti-symmetry with respect to angle, ϕ.

5.1.2 Distribution of Stress Along Radial Distance

The distributions of stress in the singular field for the two-phase anisotropic elastic bonded structure are obtained using finite element method. Figures 5.4 to 4.9 demonstrates the distributions of stresses, $\sigma_{\theta\theta}$, $\sigma_{r\theta}$, $\sigma_{\phi\theta}$ against radial distance, r on the interface of anisotropic bonded joint.

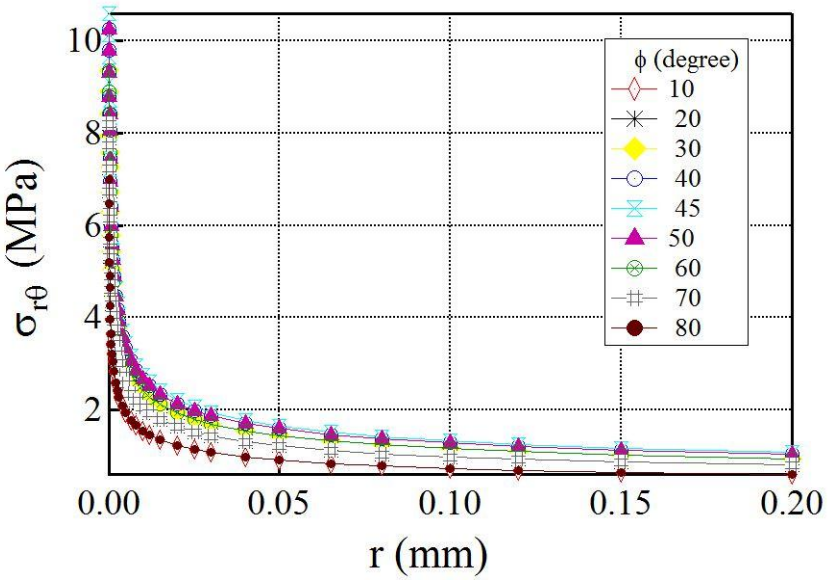

Figure 5.4: Distribution of stress, $\sigma_{r\theta}$ against r at interface

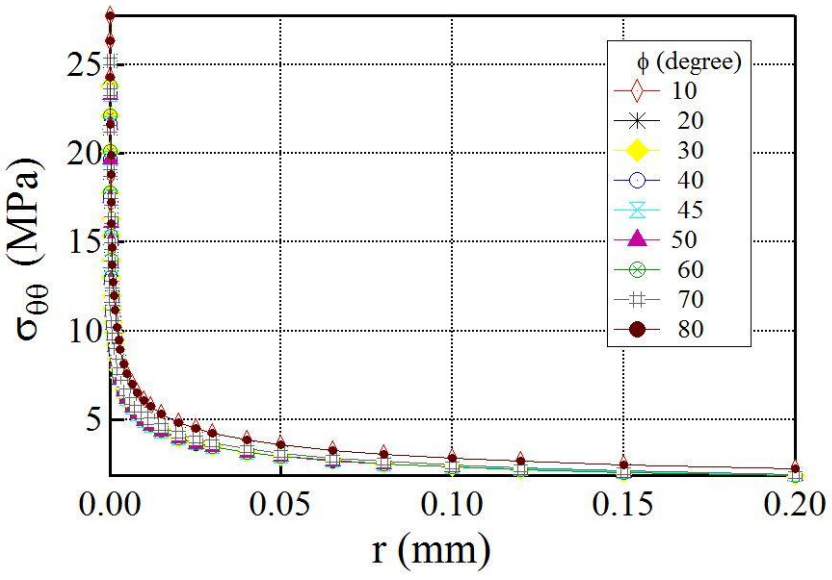

Figure 5.5: Distribution of stress, $\sigma_{\theta\theta}$ against r at interface

The above figures are plotted against radial distance, r for angle ϕ from 10° to 80°. The graphs are plotted in normal scale. All the graph show that the value of stress increases rapidly near

the vertex of the interface of anisotropic bonded joints. The interface of the joint at angle, θ = 90°.

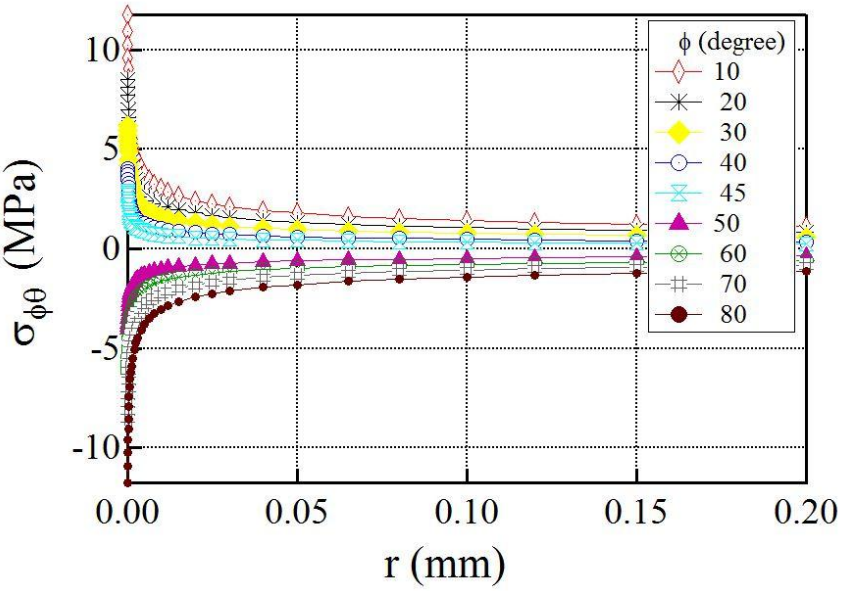

Figure 5.6: Distribution of stress, $\sigma_{\phi\theta}$ against r at interface

The value of stresses $\sigma_{r\theta}$ and $\sigma_{\theta\theta}$ are symmetry against angle ϕ and $\sigma_{\phi\theta}$ is anti-symmetry against angle ϕ. The value of stress increased rapidly with decreases of radial distance, r. Larger value of stress concentration occurs at the vertex of the joint due to stress singularity. The entire graph shows the same nature as shown in the paper of Koguchi and Costa. So there is a possibility of debonding and delamination occurs near the vertex of the joint.

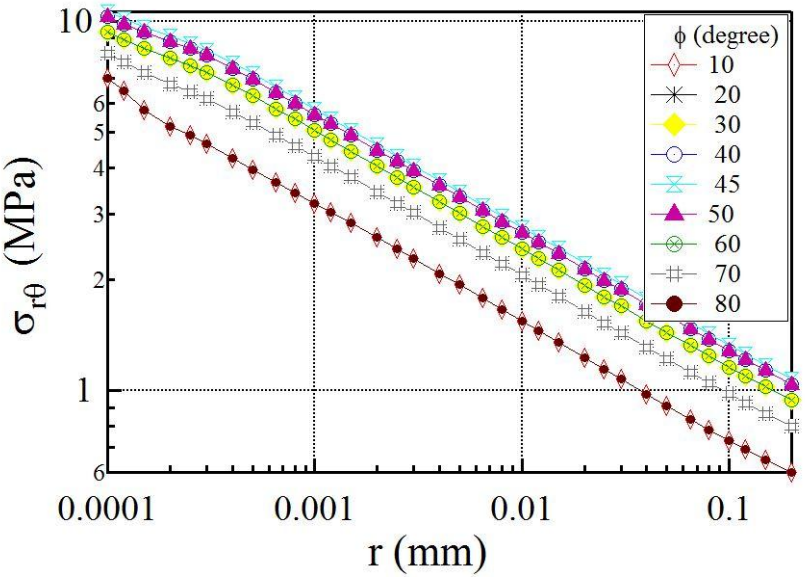

Figure 5.7: Distribution of stress, $\sigma_{r\theta}$ against radial distance r at interface

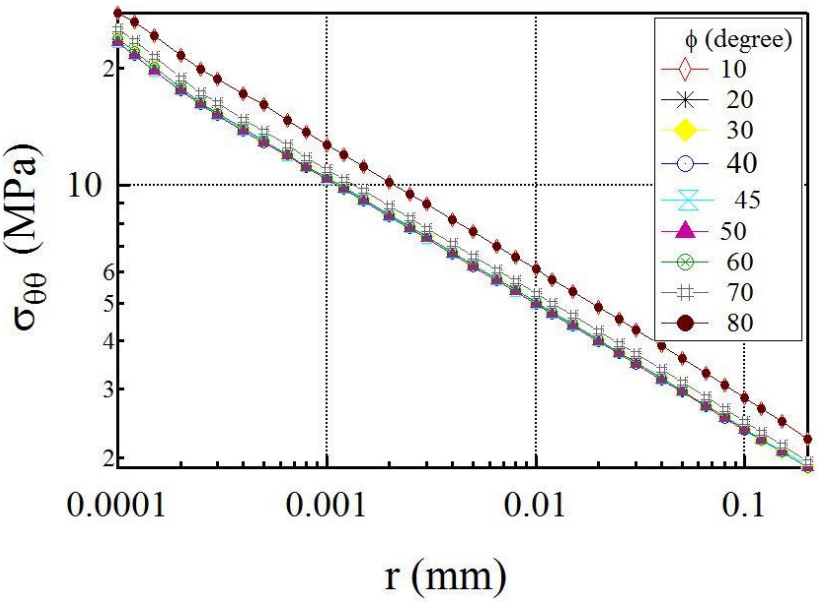

Figure 5.8: Distribution of stress, $\sigma_{\theta\theta}$ against radial distance r at interface

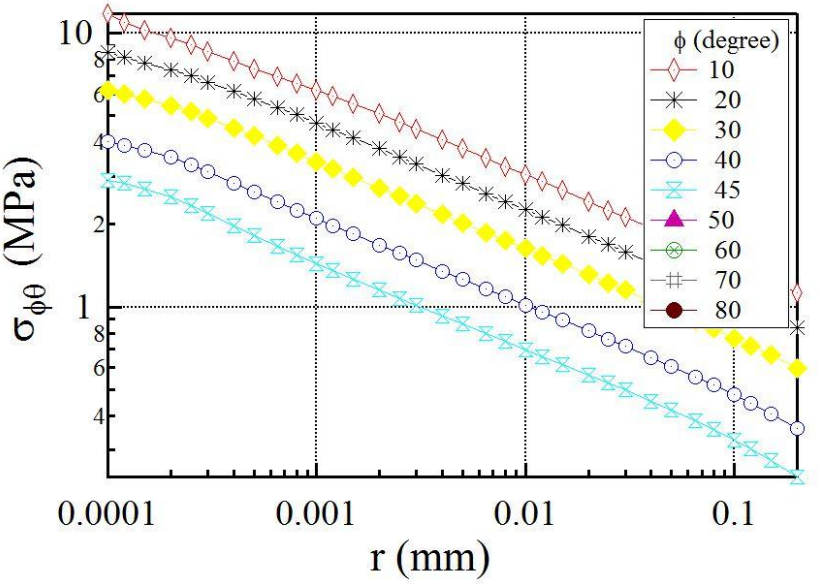

Figure 5.9: Distribution of stress, $\sigma_{\phi\theta}$ against radial distance r at interface

Here, the graphs are plotted in log-log scale. All of these graph also shows that the value of stress increases rapidly near the vertex of the joints. The value of stress $\sigma_{\phi\theta}$ is anti-symmetry against angle ϕ, therefore the stress distribution above 45° is not shown in fig. 5.9. The graphs are plotted for analyzing the stress concentration near the corner of the interface. For getting more accurate result near the vertex, the present model need to use more fine mesh near the corner of the bonded joint. The nature of the graph is compared with result of Michele, Paolo and Marino by using Ansys_Version 13 software package. All the figures show the actual stress concentration near the origin of the interface.

5.1.3 Distribution of Stress Along Angle, ϕ

Figures 5.10 to 5.15 shows the distributions of stresses $\sigma_{\theta\theta}$, $\sigma_{r\theta}$, $\sigma_{\phi\theta}$ with respect to the angle ϕ at $\theta = 90^{o}$ with r = 0.0002 mm to 0.1 mm. The stresses $\sigma_{r\theta}$ and $\sigma_{\theta\theta}$ are symmetry against angle ϕ and $\sigma_{\phi\theta}$ is anti-symmetry against angle ϕ. Figures 5.10 to 5.12 shows the distributions of stresses have larger value near the free edge of bonded joint.

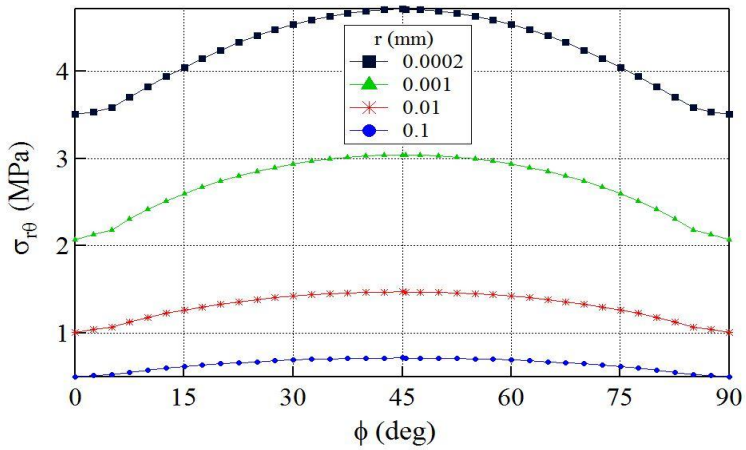

Figure 5.10: Distribution of stress, $\sigma_{r\theta}$ against angle ϕ at interface

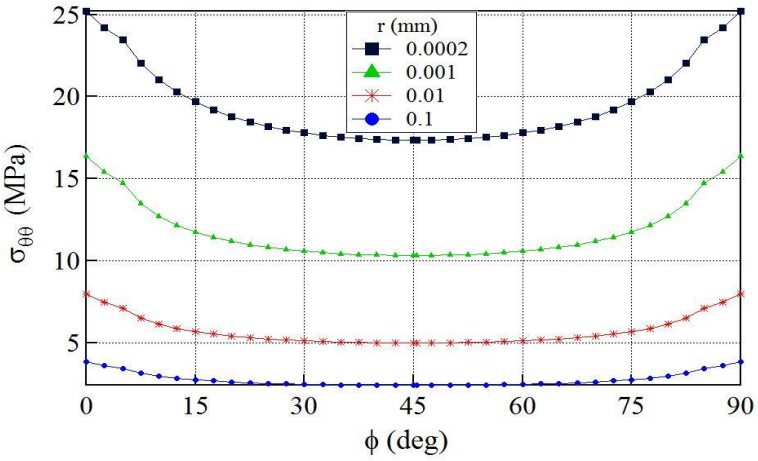

Figure 5.11: Distribution of stress, $\sigma_{\theta\theta}$ against angle ϕ at interface

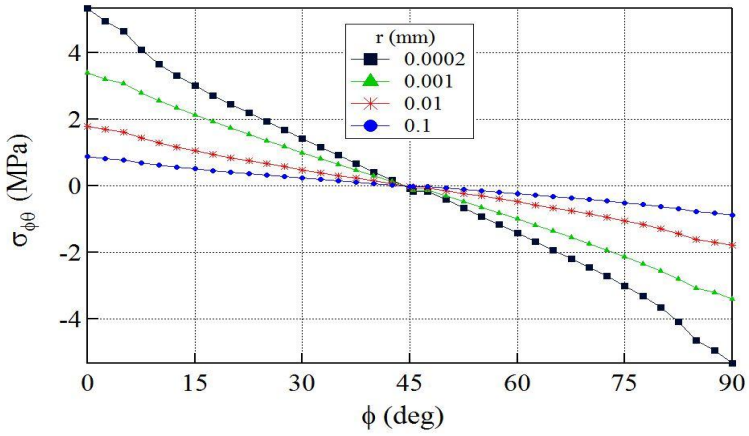

Figure 5.12: Distribution of stress, $\sigma_{\phi\theta}$ against angle ϕ at interface

All the graphs show the stress concentration increases with decreases of radial distance. The figures are plotted for analyzing the stress concentration near the interface edge of the joint. The normal stress $\sigma_{\theta\theta}$ and shear stress $\sigma_{\phi\theta}$ shows the larger value of stress near the interface edge of the joint. This is actually due to the uniformly distributed load applied on the upper portion of bonded structure. From the numerical value, it is shown that the larger value of stress field first occurs near the vertex then the free edge of the bonded joint. Therefore, near the singularity edge, stress is also higher than the inner portion of the interface. So there is another possibility of debonding and delamination occurs near the free edge of the interface.

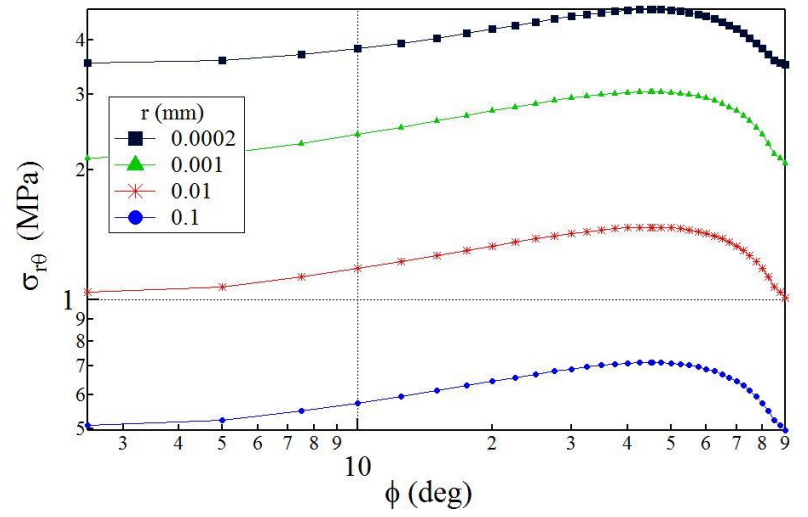

Figure 5.13: Distribution of stress, $\sigma_{r\theta}$ against angle ϕ at θ = 90°

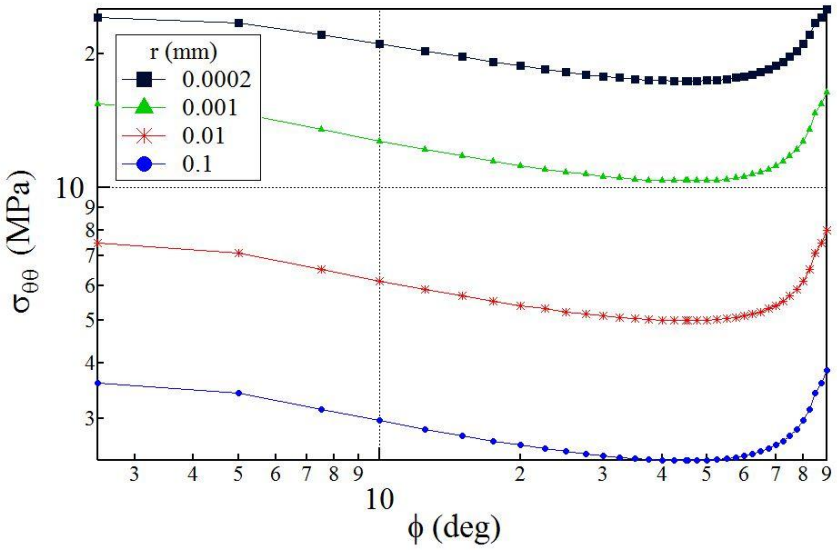

Figure 5.14: Distribution of stress, $\sigma_{\theta\theta}$ against angle ϕ at θ = 90°

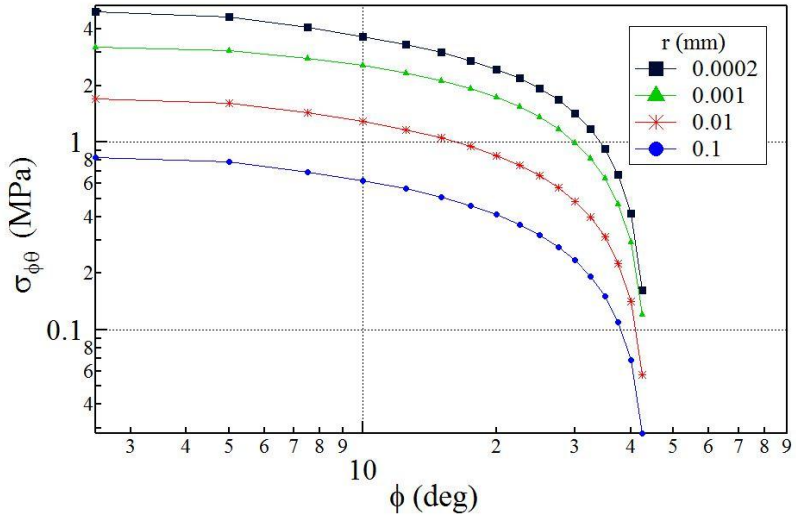

Figure 5.15: Distribution of stress, $\sigma_{\phi\theta}$ against angle ϕ at θ = 90°

Figures 5.13 to 5.15 shows the distributions of stresses $\sigma_{\theta\theta}$, $\sigma_{r\theta}$, $\sigma_{\phi\theta}$ with respect to the angle ϕ at $\theta = 90^{o}$ for various radial distance in log-log plot. The values of stress $\sigma_{\phi\theta}$ after 45° are negative. Therefore, the values of stress $\sigma_{\phi\theta}$ against ϕ, after 45° are not shown in fig. 5.15.

5.1.4 Distribution of Normalized Stress Along Angle, ϕ

Figures 5.10 to 5.15 shows the distributions of normalized stresses $\sigma_{\theta\theta}$, $\sigma_{r\theta}$, $\sigma_{\phi\theta}$ with respect to the angle ϕ at $\theta = 90^{o}$ with r = 0.0002 mm to 0.1 mm. The stresses $\sigma_{\theta\theta}$, $\sigma_{r\theta}$ are normalized by the values of stress at $\phi = \pi/2$ and $\sigma_{\phi\theta}$ is normalized by the values at $\phi = 7.5^{o}$. The stresses $\sigma_{r\theta}$ and $\sigma_{\theta\theta}$ are symmetry against angle ϕ = 45° and $\sigma_{\phi\theta}$ is anti-symmetry against angle ϕ = 45°. The value of stress $\sigma_{\theta\theta}$ is larger than the value of stresses $\sigma_{r\theta}$ and $\sigma_{\phi\theta}$. Therefore the stress $\sigma_{\theta\theta}$ is responsible for debonding and delamination near the free edge of the interface.

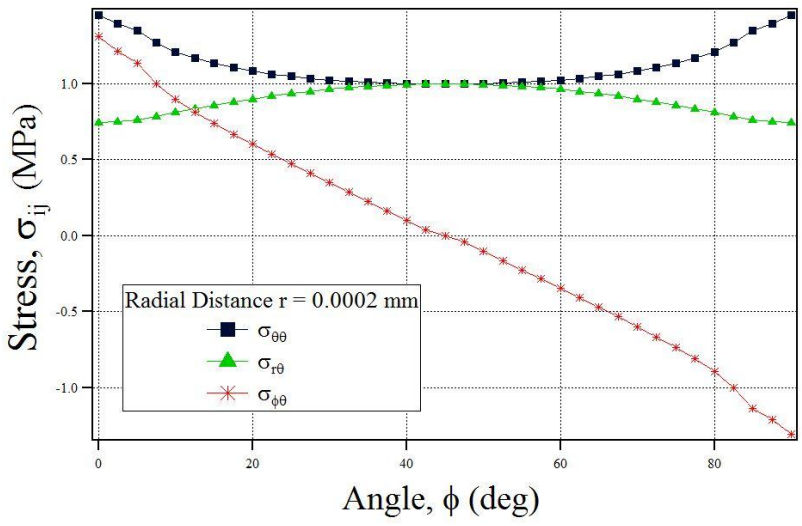

Figure 5.16: Distribution of normalized stress, σ_{ij} against angle ϕ at r = 0.0002 mm

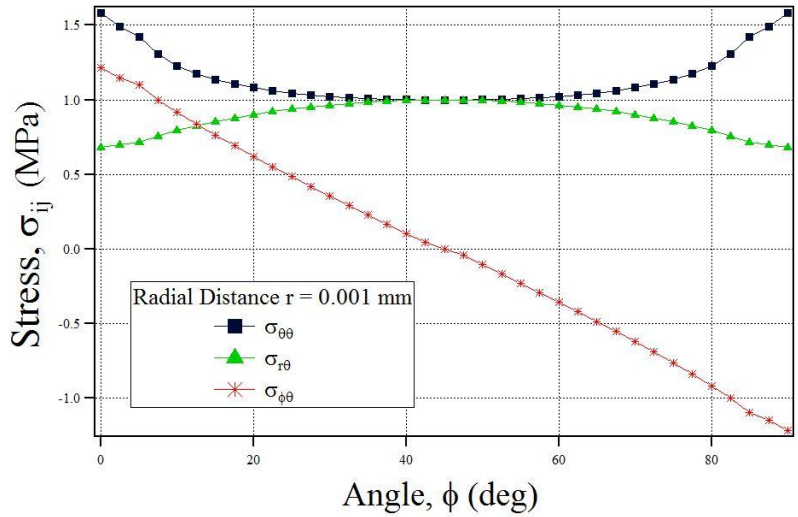

Figure 5.17: Distribution of normalized stress, σ_{ij} against angle ϕ at r = 0.001 mm

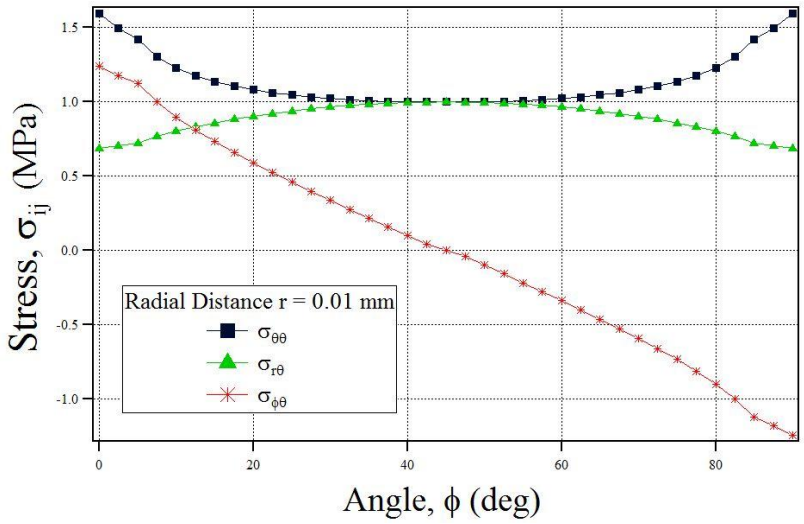

Figure 5.18: Distribution of normalized stress, σ_{ij} against angle ϕ at r = 0.01 mm

From the above figures it is shown that the curves near the angle ϕ = 0° and 90° are not so smooth. It is actually due to mesh size near the free edge of the interface. The line on the interface of present model at angle ϕ = 0° and 90° indicated the singularity line, i.e. the free edge of the bonded interface. It is not possible in the present analysis to make more fine mesh along the interface free edge, like the vertex of the interface due to low configuration computer. The normalize stress curves of this analysis are compared with the normalized curve given in the paper of Koguchi and Costa. The behavior of all the curves is similar to that given in reference [39]. More fine mesh is needed to get the smoother curve near the free edge of interface of the elastic bonded joint.

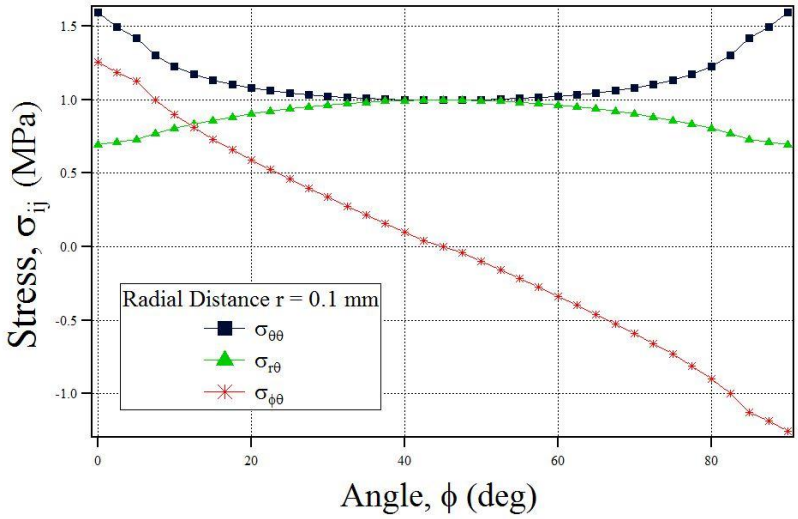

Figure 5.19: Distribution of normalized stress, σ_{ij} against angle ϕ at r = 0.1 mm

5.1.5 3D Distribution of Stress Along *r* and ϕ

Figures 5.20 to 5.22 show the three dimensional distribution of nodal stresses $\sigma_{\theta\theta}$, $\sigma_{r\theta}$, $\sigma_{\phi\theta}$ with respect to the angle ϕ and radial distance r at the interface of the joint. All the stresses have larger value near the free edge of the interface (ϕ = 0° and ϕ = 90°) and near the vertex of the joint. In the present analysis, fine meshes are use near the vertex and free edge of the interface. Therefore, the nodal stress distribution near the radial distance tense to zero is more concentrated than the other portion where the rough meshes are used.

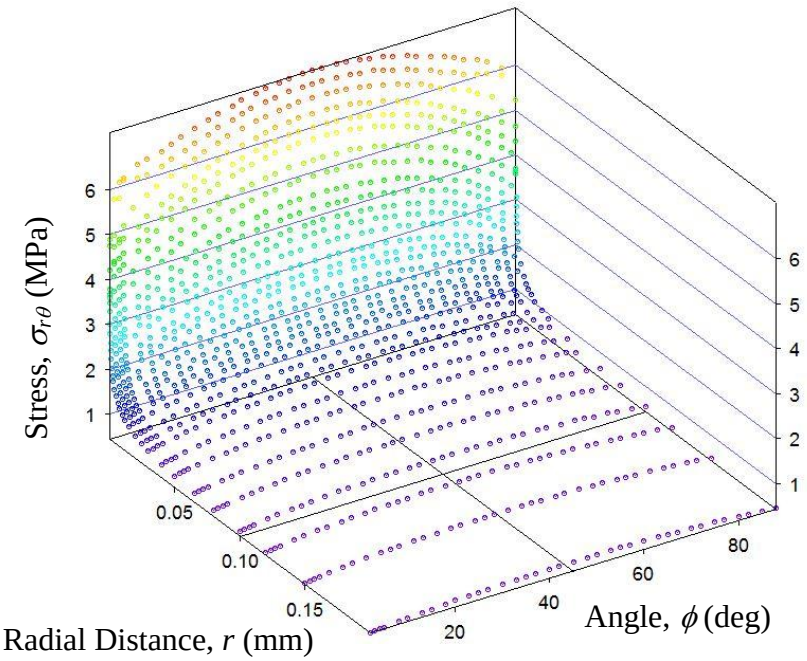

Figure 5.20: 3D distribution of nodal stress, $\sigma_{r\theta}$ against angle ϕ and radial distance r

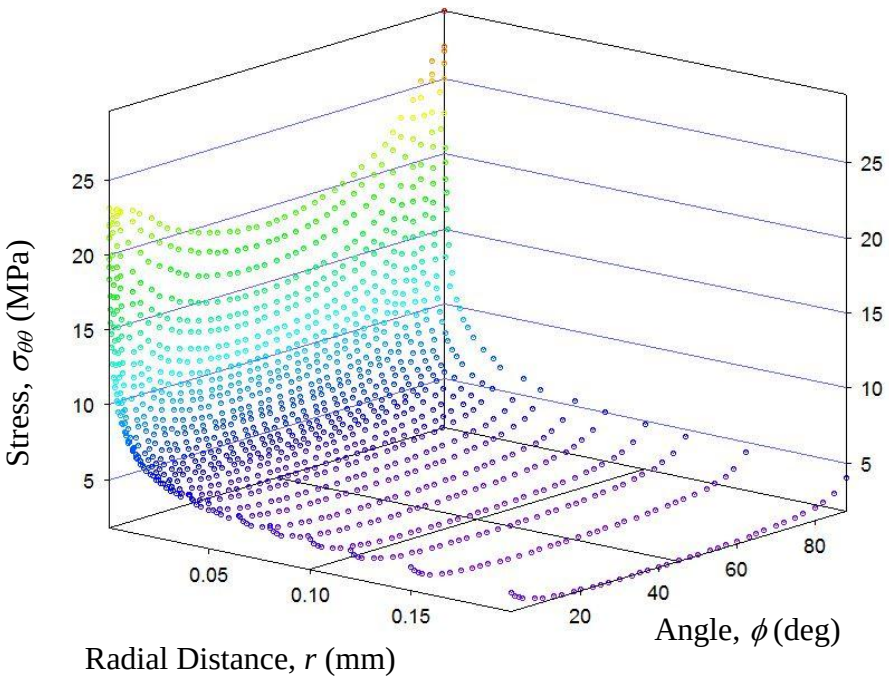

Figure 5.21: 3D distribution of nodal stress, $\sigma_{\theta\theta}$ against angle ϕ and radial distance r

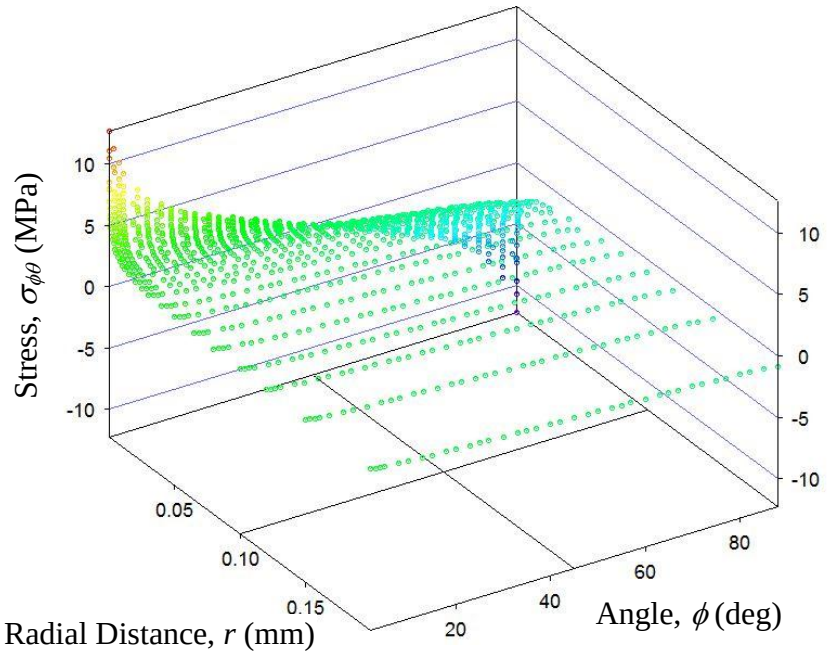

Figure 5.22: 3D distribution of nodal stress, $\sigma_{\phi\theta}$ against angle ϕ and radial distance r

5.1.6 Surface plot of displacement and Stress Along *r* and ϕ

The plot of displacement fields on the r - ϕ plane in spherical coordinates are shown in Figs. 5.23 to 5.25. Figure shows the map of elastic displacement of anisotropic elastic bonded joint of silicon and resin in surface plot. All of these graphs show the map of elastic displacement at the interface. The interface of the joint is at $\theta = 90^{o}$.

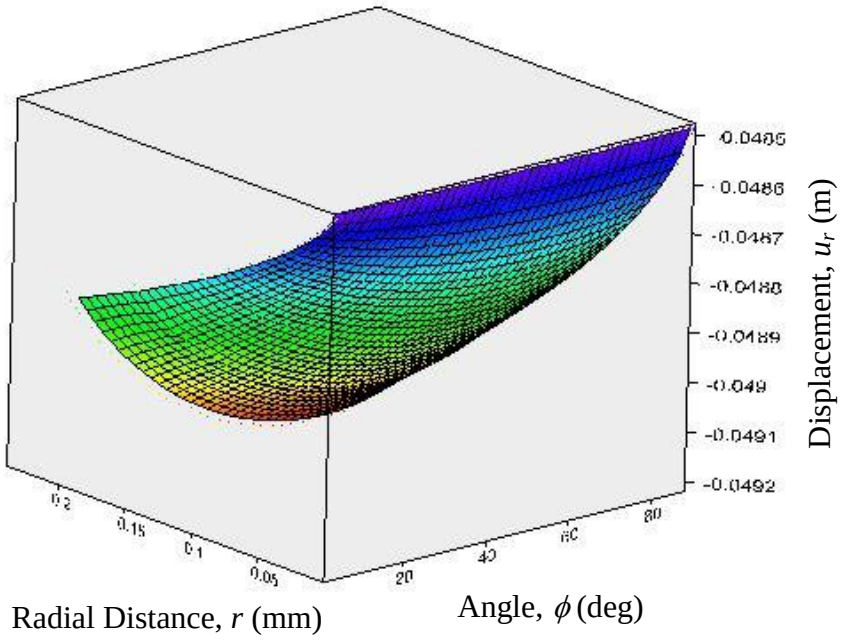

Figure 5.23: Plot of elastic displacement, u_r against r and ϕ at interface

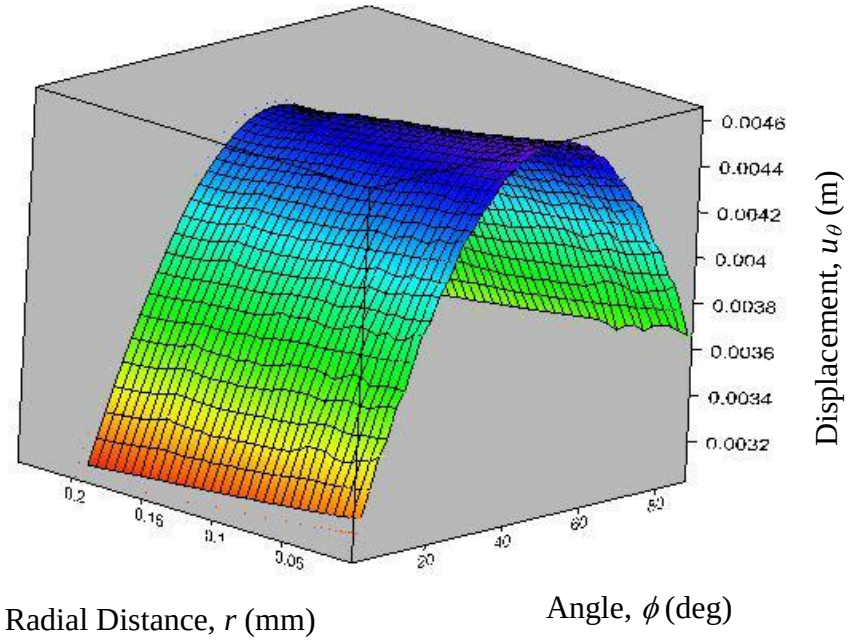

Figure 5.24: Plot of elastic displacement, u_θ against r and ϕ at interface

All the figures of surface plot are showed the same nature of nodal displacement at interface. The surface plots of displacement are not so smooth near the edge due to the rough mesh near the free edge. From the figures, it is found that, the elastic displacement is continuous at the interface of the joint and had higher value at the free edge than the inner portion. So there is a possibility to debond the joint near the free edge of the joint.

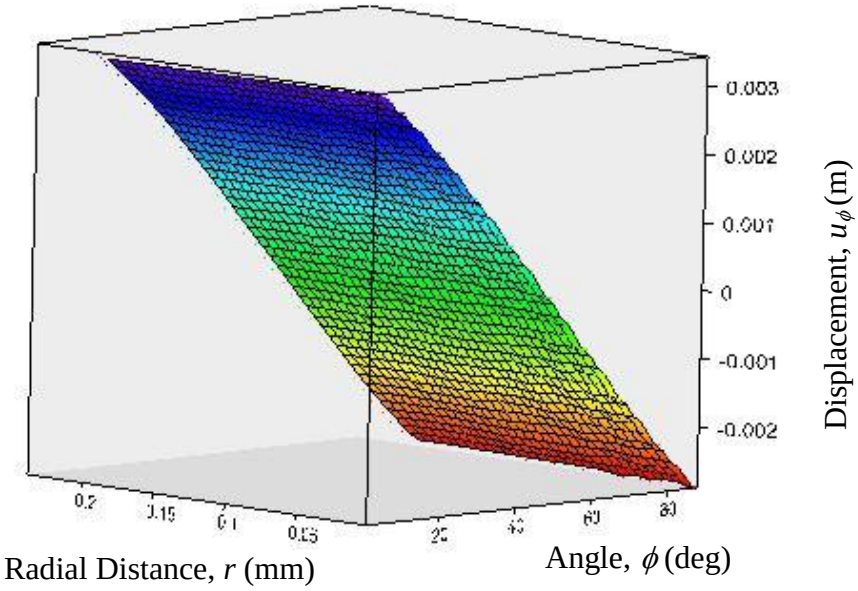

Figure 5.25: Plot of elastic displacement, u_ϕ against r and ϕ at interface

Figures 5.26 to 5.28 show the map of stresses $\sigma_{\theta\theta}$, $\sigma_{r\theta}$, $\sigma_{\phi\theta}$ with respect to the angle, ϕ and radial distance, r at the interface of the joint in surface plot. The figures of surface plot are also showed the same nature as nodal stress at interface. It is shown from the graphs that there is more noise near the free edge. More fine mesh is needed near the interface edge to avoid the noise at the free edge. The normal stress $\sigma_{\theta\theta}$ and shear stress $\sigma_{\phi\theta}$ shows the larger value of stress near the interface edge of the joint.

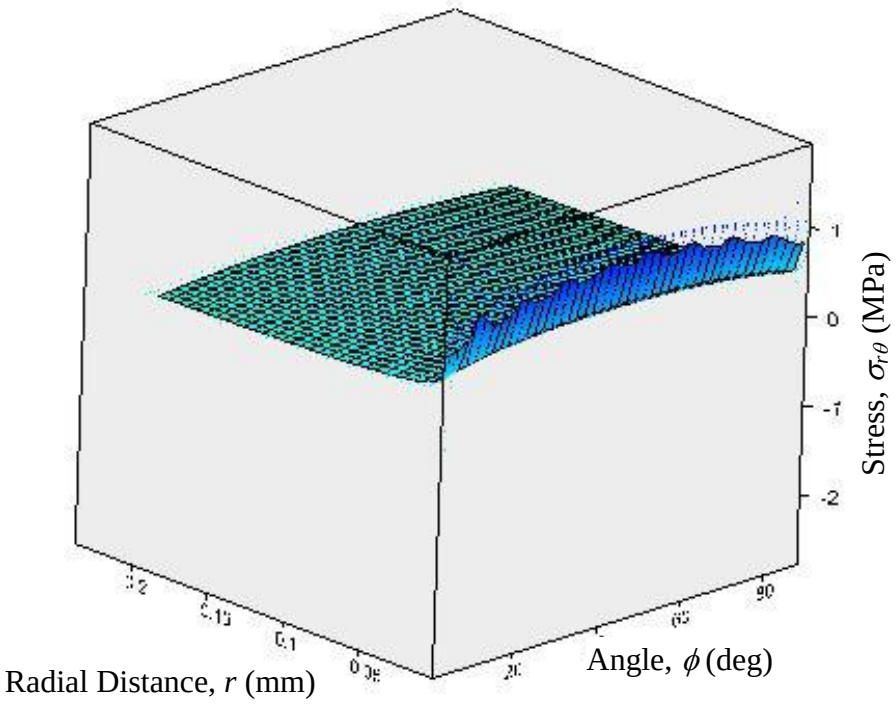

Figure 5.26: Map of stress, $\sigma_{r\theta}$ against angle, ϕ and radial distance, r

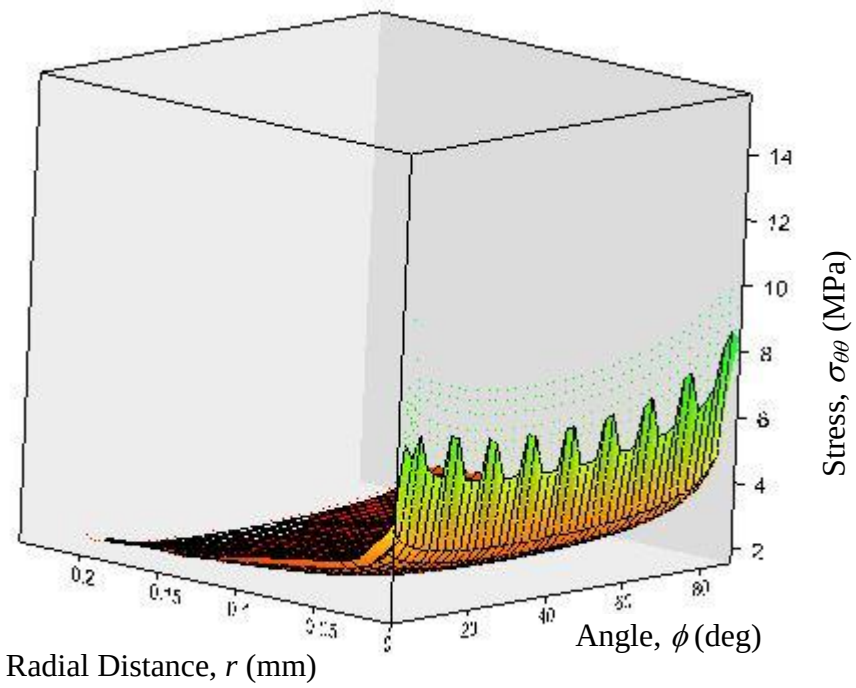

Figure 5.27: Map of stress, $\sigma_{\theta\theta}$ against angle, ϕ and radial distance, r

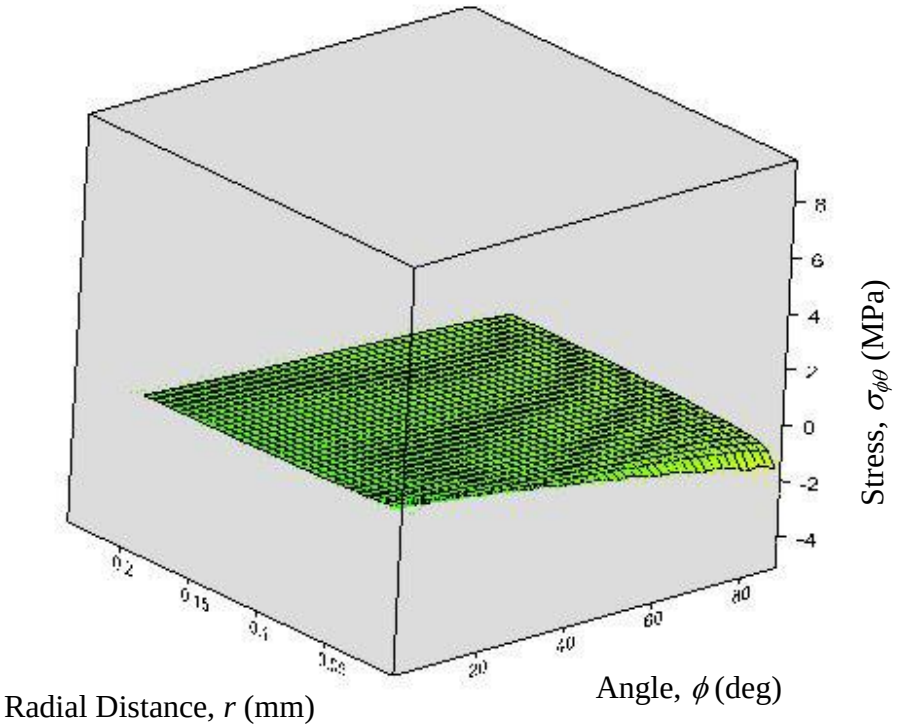

Figure 5.28: Map of stress, $\sigma_{\phi\theta}$ against angle, ϕ and radial distance, r

It is also found that the stress at $\phi = 0°$ is agreed with that at $\phi = 90°$. The $\sigma_{\theta\theta}$ and $\sigma_{r\theta}$ graph are symmetry with respect to angle, ϕ and $\sigma_{\phi\theta}$ is anti-symmetry with respect to angle, ϕ. These surface plots are agreed with the result of 2D stress distribution. All the stresses have larger value near the free edge of the interface ($\phi = 0°$ and $\phi = 90°$) and near the vertex of the joint.

5.2 Discussions

The failure of dissimilar material joint may be caused by a mismatch of material properties such as mechanical, electrical and thermal properties. Delamination and debonding may occur at the interface free edges. Failures in engineering applications of bonded materials are caused by this reason. Therefore, displacement and stress fields near the interface free edge become an important topic to study the failure in dissimilar material joints by many authors.

The characteristics of stress and displacement field around the vertex has been considered and defined as many parameters such as eigen value, the order of singularity, the stress intensity factor for crack problems and the intensity of singularity for joint problems. The stress field at the vertex in anisotropic dissimilar material joints is calculated from the combination of material properties in numerical method. The material properties are often used for considering the crack growth and the occurrence of delamination and debonding.

Different numerical methods had developed for determining the stress field in a three-dimensional anisotropic elastic dissimilar material joint. In this study, the stress field at a vertex in 3D anisotropic dissimilar material joints was investigated using a finite element analysis. The distributions of stress and displacement with respect to radial distance, r and angle, ϕ were calculated using FEM. The stress and displacement distributions near the vertex on the boundaries in a Cartesian coordinate were converted to express the inner stress and displacement distributions in a spherical coordinate. The stress and displacement have a larger value at the vertex and near the free edge of the joint. Therefore, there is a possibility to debond and delamination at the corner and the interface edge of the bonded joints.

CHAPTER VI

Conclusion and Future work

6.1 Conclusions

In this thesis paper, a finite element method formulation near the vertex and free edge of anisotropic elastic bonded joint was presented. The distributions of stress and elastic displacement were investigated using Autodesk Simulation Mechanical 2015 student version based on a finite element method. From the numerical result, the following conclusions can be drawn for the anisotropic bimaterial joints.

(1) The higher elastic displacement occurs at the corner and free edge of the material joint than the inner portion of the joint.
(2) The larger stress field developed near the corner and free edge of the anisotropic elastic bonded joints.
(3) The stress $\sigma_{\theta\theta}$ is larger than other stresses developed at the corner and free edge of the material joint.
(4) The possibility of debonding and delamination occurs near the corner and free edge of the anisotropic elastic bonded joints was due to the higher stress concentration.

6.2 Future work

In the present analysis used Autodesk Simulation Mechanical 2015 software based on FEM. The future work will carried out with BEM and FVM. The research work is carried out only anisotropic material of silicon and resin. But the bonded joint use isotropic, anisotropic and transversely isotropic of different materials. The present analysis was carried out on the basis of model shown in figure 4.1. But this model is very simple and fine mesh was not used near the interface edge. For that reason future work will be carried out with more complex and used more fine mesh near the vertex and along the free edge. The different combination of material joints with more fine mesh will have the following objectives for future work.

1. To determine the order of stress singularity.
2. To determine the distribution of elastic displacement.
3. To determine the strain material joints.
4. To determine the distribution of stress components

REFERENCES

1 Tsukada Y., Nishimura H., Sakane M. and Ohnami M., 2000, "Fatigue Life Analysis of Solder Joints in Flip Chip Bonding", Journal of Electronic Packaging, Vol. 122, pp. 207-213.

2 Zhang X., Lee R. S-W. and Pao Y-H., 2000, "A Damage Evolution Model for Thermal Fatigue Analysis of Solder Joints", Transactions of the ASME, Vol. 122, pp. 200-206.

3 Su B., Lee Y. C. and Martin L. D., 2000, "Die Cracking at Solder (In60-Pb40) Joints on Brittle (GaAs) Chips: Fracture Correlation Using Critical Bimaterial Interface Corner Stress Intensities", Journal of Electronic Packaging, Vol. 125, pp. 369-377.

4 Charlie Z. J., Sidharth, Richard B., Raj M. and Srinivaran P., 2003, "Interfacial Fracture Analysis of Underfill Delamination and Flip Chip Reliability Optimization", IEEE, pp. 714-719.

5 Williams M. L., 1952, "Surface Stress Singularities Resulting From Various Boundary Conditions in Angular Corners of Plates under Bending", Proceedings, First U.S. National Congress of Applied Mechanics, ASME, pp. 325-329.

6 Williams M. L., 1959, "The Stress Around a Fault or Crack in Dissimilar Media", Bulletin of the Seismological Society of America, Vol.49, pp. 199-204.

7 Zak A. R. and Williams M. L., 1963, "Crack Point Stress Singularities at a Bi-Material Interface", Journal of Application Mechanics, Trans. ASME, Brief Notes, pp. 142-143.

8 Aksentian O. K., 1967, "Singularities of the Stress-Strain State of A Plate in The Neighborhood of An Edge", PMM, Vol.31-1, pp.178-186.

9 Dundurs J., 1969, "Discussion of Edge-Bonded Dissimilar Orthogonal Elastic Wedges under Normal and Shear Loading", Journal of Application Mechanics, Vol.36, pp. 650-652.

10 Bogy D. B., 1971, "Two Edge-Bonded Elastic Wedges of Different Materials and Wedge Angles under Surface Tractions", Journal of Applied Mechanics, ASME, Vol.38, No.2, pp. 377-386.

11 Bogy D. B., Wang K. C., "Stress Singularities at Interface Corners in Bonded Dissimilar Isotropic Elastic Materials", Int. Journal of Solid Structures, Vol. 7, November, 1971, pp. 993-1005.

12 Kawai T., Fujitani Y. and Kobayashi M., 1977, "Stress Analysis of the Conical Surface Pit Problem", Proc. Int. Conference of Fracture Mechanic and Technology,

Hong Kong, Vol.2, pp.1165-1170.

13 Kawai T., Fujitani Y. and Kumagai K., 1977, "Analysis of Singularity at the Root of the Surface Crack Problem", Proc. Int. Conference of Fracture Mechanic and Technology, Hong Kong, Vol.2, pp.1157-1163.

14 Benthem J. P., 1980, "The Quarter-Infinite Crack in a Half-Space; Alternative and Additional Solutions", Int. Journal of Solid Structures, Vol. 16, pp. 119-130.

15 Dempsey J. P. and Sinclair G.B., 1979, "On the Stress Singularities in the Plane Elasticity of the Composite Wedge", Journal of Elasticity, Vol.9-4, pp. 373-391.

16 Dempsey J. P., 1995, "Power-Logarithmic Stress Singularities at Bi-Material Corners and Interface Cracks", Journal of Adhesion Science and Technology, Vol. 9-2, pp. 256-265.

17 Bazant Z. P. and Estenssoro L. F., 1979, "Surface Singularity and Crack Propagation", Int. Journal of Solid Structures, Vol. 15, pp. 405-426.

18 Yamada Y. and Okumura H., 1981, "Analysis of Local Stress in Composite Materials by the 3-D Finite Element", In Proc. Japan-U.S.A. Conference (Edited by K. Kawata and T. Akasaka), pp.55-64.

19 Pageau S. S., Joseph P. F. and Biggers Jr S. B., 1995, "Finite Element Analysis of Anisotropic Materials with Singular Inplane Stress Fields", Int. Journal of Solid Structures, Vol. 32, pp.571-591.

20 Pageau S. S. and Biggers Jr S. B., 1995, "Finite Element Evaluation of Free-Edge Singular Stress Fields in Anisotropic Materials", Int. Journal for Numerical Methods in Engineering, Vol. 38, pp. 2225-2239.

21 Pageau S. S., Joseph P. F. and Biggers Jr S. B., 1996, "A Finite Element Approach to Three-Dimensional Singular Stress States in Anisotropic Multi-Material Wedges and Junctions", Int. Journal of Solid Structures, Vol. 33, pp. 33-47.

22 Koguchi H., 1996, "Stress singularity analysis in three-dimensional bonded structure", Int. Journal of Solid Structures, Vol. 34, pp. 461-480.

23 Koguchi H., 2006, "Stress singularity analysis in three-dimensional bonded structure", Transactions of the JSME, Vol. 72, No. 724-A, pp. 2058-2065..

24 Leblond J. B. and Leguillon D., 1999, "The stress intensity factors near an angular point on the front of an interface crack", European Journal of Mechanics and Solids, Vol. 18, pp. 837-857.

25 Dimitrov A., Andra H. and Schnack E., 2001, "Efficient computation of order and mode of corner singularities in 3D-elasticity", Int. Journal for Numerical Methods in Engineering, Vol. 52, pp. 805-827.

26 Dimitrov A., Andra H. and Schnack E., 2002, "Efficient computation of order and mode of corner singularities in 3D-elasticity", Int. Journal of Fracture, Vol. 115, pp. 361-375.

27 Lee Y. and Im S., 2003, "On the computation of the near-tip stress intensities for three-dimensional wedges via two-state M-integral", Journal of Mechanics physics and Solids, Vol. 51, pp. 825-850.

28 Apel T., Leguillon D., Pester C. and Yosibash Z., 2008, "Edge singularities and structure of the 3-D Williams expansion", C R Mecanique, Vol. 336, pp. 629-635.

29 Yosibash Z., Omer N., and Dauge M., 2008, "Edge stress intensity functions in 3-D anisotropic composites", Composites Science and Technology, Vol. 68, pp. 1216-1224.

30 Omer N., and Yosibash Z., 2008, "Edge singularities in 3-D elastic anisotropic and multi-material domains", Computer Methods in Applied Mechanics and Engineering, Vol. 197, pp. 959-978.

31 Hrennikoff A., 1941, "Solution of Problems of Elasticity by the Frame-Work Method", Journal of Application Mechanics, Trans. ASME, pp. 619-715.

32 Courant R. L., 1943, "Variational Methods for the Solution of Problems of Equilibrium and Variation", Bulletin of the American Mathematical Society, Vol.49, No. 1, pp. 1-23.

33 Clough R. W., 2004, "Early History of the Finite Element Method from the View Point of a Pioneer", International Journal for Numerical Methods in Engineering, Vol.60, pp. 283-287.

34 Turner M. J., Clough R. W., Martin H. C. and Topp L., 1956, "Stiffness and Deflection Analysis of Complex Structure", Journal of Aeronautical Sciences, Vol.23.

35 Clough R. W., 1960, "The Finite Element Method in Plane Stress Analysis", Procedures of the Second ASCE Conference on Electronic Computation, Pittsburgh, PA.

36 Clough R. W., 1962, "Stress Analysis of a Gravity Dam by the Finite Element Method", Proceeding of the Symposium on the Use of Computers in Civil Engineering, Laboratorio Nacional de Engenharia Civil, Lisbon, Portugal.

37 Clough R. W., 1965, "The Finite Element Method in Structural Mechanics", Stress Analysis, Chapter 7, Wiley: Newyork.

38 Kollar L. P. and Springer, G. S., 2003 “Mechanics of Composite Structures”, University of Cambridge, USA.

39 Koguchi H. and Costa J. A., 2010, “Analysis of the stress singularity field at a vertex in 3D-bonded structures having a slanted side surface”, Int. Journal of Solid Structures, Vol. 47, pp. 3131-3140.

40 Michele Z., Paolo A. C., and Marino Q., 2015 “Analytical solution for the three-dimensional stress fields in anisotropic composite bimaterial corners”, Composite Structures, Vol. 122, pp. 127-138.